People's Democratic Republic of Algeria
Ministry of Higher Education and Scientific Research

Ibn Khaldoun University – Tiaret
Faculty of Applied Sciences
Department of Mechanical Engineering

Dissertation submitted in order to obtain the Master's Degree in the Field of Mechanical Engineering

Domain: Sciences and Technology

Field: Mechanical Engineering

Specialty: Energetic

Titled:

Numerical study of viscoplastic flow through a sudden expansion

Presented by:

MIMOUN Fatma and KADAOUI Selma

Publicly defended on: 12/06/2024

Board of Examiners

Names	Grade	University of Reattachment	Quality
SAID Mekroussi	Pr	University of Tiaret	President
SAD CHEMLOUL Nord-Eddine	Pr	University of Tiaret	Supervisor
KARAS Abdelkader	Pr	University of Tiaret	Examiner
BELMILOUD Mohamed Amine	MCB	University of Tiaret	Examiner

Academic Year: 2023/2024


بسم الله الرحمن الرحيم

Dedication

In loving memory of my grandfather, ***MIMOUN Taher****.*

I dedicate this work.

MIMOUN Fatma

Dedication

To my late father, God rest his soul.

To my dear mom and aunt to my whole family.

To all those who are dear to me.

To all my friends.

I dedicate the fruit of my 17 years of studies.

KADAOUI Selma

Acknowledgements

In the name of Allah, the most Gracious, the most Merciful. All thanks to Allah, the Lord of both worlds, and may prayers and peace be upon our Prophet, Muhammad and upon his companions. We would like to express our sincere gratitude to our esteemed supervisor, Professor ***SAD CHEMLOUL Nord-Eddine*** *of Ibn Khaldoun University of Tiaret, for his invaluable guidance and dedicated facilitation throughout this work*

We extend our deepest gratitude to ***Dr. BEKHADRA Mokhtar*** *for his invaluable contribution at every stage of this research.*

we sincerely thank all the members of the jury ***(Pr. SAID Mekroussi, Pr. KARRAS Abdelkader and Ms. BELMILOUD Mohamed Amine)*** *for diligently fulfilling their roles and supervising this thesis. Your presence and contributions are deeply appreciated.*

We wish to extend our heartfelt thanks to the Department of Mechanics at Tiaret University, particularly ***Ms. ABOUCHGHAIBA Hichem****, for the invaluable advice he has provided over the past two years. His guidance has significantly impacted our education.*

This Dissertation would not have been possible without the unwavering support of our friends, everyone who believed in us. And ***INNOVATION CLUB****, we are incredibly grateful for your encouragement and assistance throughout this journey.*

And last but not least, we would highly appreciate the efforts devoted by our parents all our educational stages.

Summary

Chapter IV: Results and discussions

List of figures

List of Tables

Latin's Symbols

D_{ij}	Rate of deformation.
F	Force applicated [N].
K	Consistency index $Pa.s^n$.
L	Length of the channel [m].
L_1	Length of the small channel [m].
L_2	Length of the large channel [m].
L_v	Vortex length [m].
R	Radius of the channel [m].
R_1	Radius of the small channel [m].
R_2	Radius of the large channel [m].
S	Area of sheared layer [m^2].
U_i	Inlet velocity [m/s].
d	Diameter of the channel [m].
n	Power-law index.
r	Radiale coordinate.
r_c	Critical radius [m].
u	Axial velocity [m/s].
x	Axial coordinate.
Y	Yield number $\tau_y d^n / K U_i^n$
z	Transverse coordinate.

Greeks Symbols

Δp_L	Major head loss.
Δp_s	Minor head loss.
ψ^*	Vortex Intensity.
τ	Shear stress [Pa].
τ_y	Yield stress.

ρ	Density of fluid [Kg/m^3].
γ	Deformation.
$\dot{\gamma}$	Shear rate [s^{-1}]
λ	Fluid-specific constants defining the shape of the viscosity curve as a function of shear rate.
μ_p	Viscosity of the fluid.

Dimensionless Numbers

Bn	Bingham Number.
He	Hedstrom number.
Re	Reynolds Number.

Abbreviations

CFD	Computational Fluid Dynamics.
FVM	Finite Volume Method.
PDEs	Partial Differential Equations.
DBCS	Density-Based Coupled Solver.

General Introduction

In the field of fluid mechanics, understanding the flow of viscoplastic fluids through complex geometries is crucial, both theoretically and practically. Viscoplastic fluids are a class of materials exhibiting complex flow behavior, combining viscous and plastic characteristics. They are encountered in various industrial processes, including food processing, paints, and slurries. A wide range of these complex structured fluids are now used in industry and the manufacture of an increasing number of products for a wide range of industries: food, pharmaceutical, chemical, polymer, hydrocarbon transport and natural gas treatment, in addition to applications in the oil, mining, construction, water treatment and energy production industries. The majority of fluids in everyday life exhibit non-Newtonian rheological behavior, making Newtonian fluid behavior the exception rather than the rule.

This work focuses on the numerical simulation of laminar flow of a Viscoplastic fluid (Bingham and Hershel-Bulkley) through an axisymmetric sudden expansion.

The present work is divided into four chapters, each dealing with essential aspects of the problem studied. The first chapter is dedicated to a thorough review of rheology, highlighting the distinction between Newtonian and non-Newtonian fluids. Fundamental concepts such as dimensionless numbers, including the Bingham and Reynolds numbers, are discussed.

The second chapter focuses on the geometry of the sudden expansion and presents the mathematical formulations necessary to model this complex flow. It also includes an analytical solution for the problem of fluid flow in a cylindrical pipe under laminar flow.

The third chapter focuses on the chosen numerical method to simulate the flow, which is the commercial code ANSYS Fluent.

In the fourth chapter, we performed a dynamic validation which consists of comparing experimental and numerical works in the literature with our results, followed by a presentation of the axial velocity fields, streamlines representing the vortex zones and shear stress contours representing the solid zones in the flow. The results obtained on the pressure drop coefficient for this type of fluid are also presented.

This study aims to contribute to the understanding of the behavior of viscoplastic fluids through sudden expansions. The acquired knowledge can be valuable for engineers working

with these materials in various industrial applications. The main results are presented in the general conclusion of this numerical study.

Chapter I
Bibliographic study

Introduction

Understanding how fluid flows through expansion is crucial in various engineering applications, from designing efficient pipelines to optimizing blood flow in the human body. Imagine blood flowing smoothly through a widening artery or air moving through a vent. These relatable examples highlight the importance of fluid flow through expansion. Existing models provide a good foundation, but challenges remain in predicting behavior under specific conditions.

The following sections will guide us through the literature review, theoretical background, and details of our work approach. We will delve into past research on fluid flow through expansion and place our work in the context of other literary works.

I.1 Fluid definition:

A fluid is defined as any substance that exhibits continuous flow and deformation when subjected to shear stress or external force. Under permanent deformation, fluids lose their distinct form and instead take on the shape of the container that holds them [1].

While some fluids, like water, demonstrate high fluidity, there exists a spectrum of viscosity among substances. For instance, pastes, paints, jelly, and concentrated polymer solutions are considerably more viscous. These materials can behave as liquids for prolonged periods, yet intermittently display solid-like properties.

The dynamic nature of fluids is further highlighted by their ability to adjust to different environmental conditions. Fluids not only adapt to the shape of their container but also vary in their flow characteristics. Some exhibit a remarkable ability to transition between liquid and solid states, emphasizing the complexity and versatility inherent in the behavior of fluids. This distinctive property makes fluids a fascinating area of study with applications ranging from industrial processes to biological systems.

I.2 Rheological quantities:

I.2.1 Dynamic Viscosity:

Isaac Newton's development of the concept of viscosity for real fluids in 1687 was influenced by the prior experiments conducted by Robert Hooke in 1678, which focused on a solid elastic material. Newton, in his observations of fluid flow resistance, postulated that

viscosity, as the measure of a fluid's response to applied stress, is directly linked to the speed gradient. This insight underscores the idea that viscosity emerges from the exchanges of movement quantities between different layers of the fluid, a process intricately tied to the thermal molecular agitation [2]. This fundamental understanding of viscosity has since played a crucial role in fluid dynamics and continues to be a cornerstone in the study of fluid behavior.

Dynamic viscosity is given by:

$$\mu = \frac{\tau_{ij}}{\dot{\gamma}_{ij}} \tag{I.1}$$

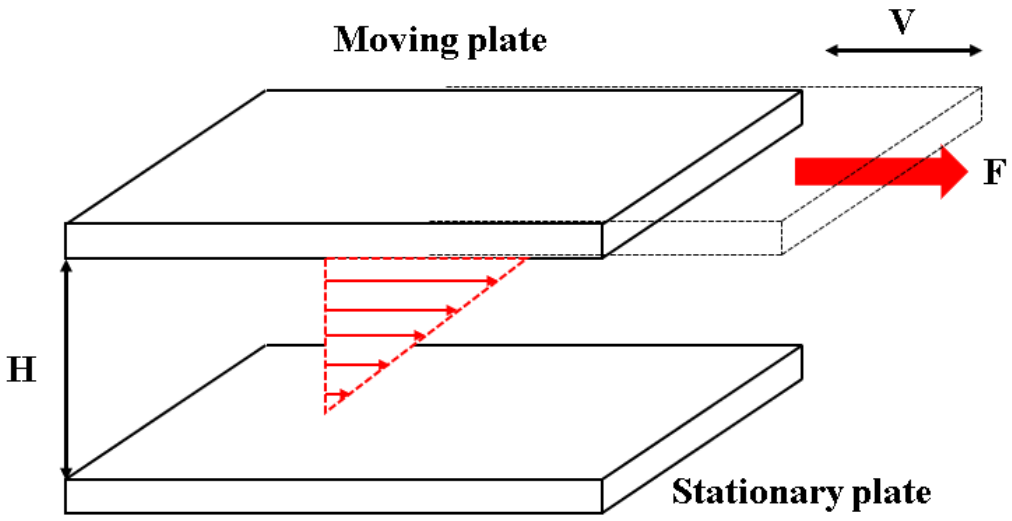

Figure I. 1: The Two-Plate-Model Definition of Viscosity [3].

The viscosity of a fluid μ measures its strain resistance when shear stress is applied. The lower the viscosity, the easier the liquid will flow, and conversely, for a high viscosity, it will flow more slowly.

Viscosity depends on several criteria:

- ✓ The type of fluid.
- ✓ Stress and shear rate.
- ✓ The temperature.
- ✓ The time.

Certain substances showcase a dependence of viscosity on shear stress and/or shear speed, classifying them as non-Newtonian fluids. In these instances, the dynamic viscosity coefficient

is termed apparent viscosity and is symbolized by μ. The rheological equation governing the behavior of these fluids is articulated as follows:

$$\tau = \mu \frac{du}{dy} \tag{I.2}$$

This equation captures the nuanced relationship between shear stress, apparent viscosity, and shear rate in non-Newtonian fluids, emphasizing the deviation from the linear relationship observed in Newtonian fluids.

I.2.2 Cinematic Viscosity:

Cinematic viscosity, although applicable to all liquids, whether they exhibit Newtonian or non-Newtonian behaviors, finds its predominant utility in the field of Newtonian liquids. It is in this specific context that a direct method of determining kinematic viscosity through capillary rheometer is revealed. This method provides a clear justification for the importance given to this coefficient in the case of liquids with fluid behavior in accordance with Newtonian laws, despite the diversity of viscoelastic characteristics that can be observed in other types of liquids. Thus, kinematic viscosity becomes a fundamental tool in the study and understanding of the rheological properties of liquids, especially in the field of Newtonian fluids.

Cinematic viscosity is given by:

$$v = \frac{\mu}{\rho} \tag{I.3}$$

I.2.3 Shear stress:

From the parallel plate experiment (Figure I.1) where the plate is moving with a velocity U, the fluid particles in contact with the moving plate will have the same speed. This velocity of the fluid particles decreases when moving towards the fixed wall where the velocity is zero.

This constraint that appears during laminar fluid movement, relative motion of layers relative to each other, results in the appearance of frictional forces which exert tangentially on the surface of the layer [4].

$$\tau_{ij} = \frac{F}{S} = \mu \frac{du_i}{dx_j} \tag{I.4}$$

I.2.4 Deformation (shear strain):

The results of the action of an external force can be either the movement of a body in space as a whole, a change in its shape. The change in the shape of a body is essentially the change of distances between different sites within a material, and this phenomenon is called deformation, deformation is only a geometric concept.

The change in distance between points inside a body can be monitored by following the change of very small distance between two neighboring points. So, we can say that the deformation γ is the ratio between the length of the deformation and the length perpendicular in the plane of the applied force[5].

In other words, it is the tangent of the deformation angle.

$$\gamma = \frac{d\xi}{dy} = \tan(\alpha) \simeq \alpha \tag{I.4}$$

I.2.5 Strain rate (shear rate):

The noted shear rate is defined as the change in deformation over time:

$$\dot{\gamma}_{ij} = \frac{d\gamma}{dt} = \frac{d}{dt}\frac{d\xi}{dx_j} = \frac{d}{dx_j}\frac{d\xi}{dt} = \frac{du_i}{dx_j} \tag{I.5}$$

The deformation rate is therefore equal to the shear rate, which in the specific situation of simple shear is the axial velocity derivative with respect to the position, as shown in Figure I.2.

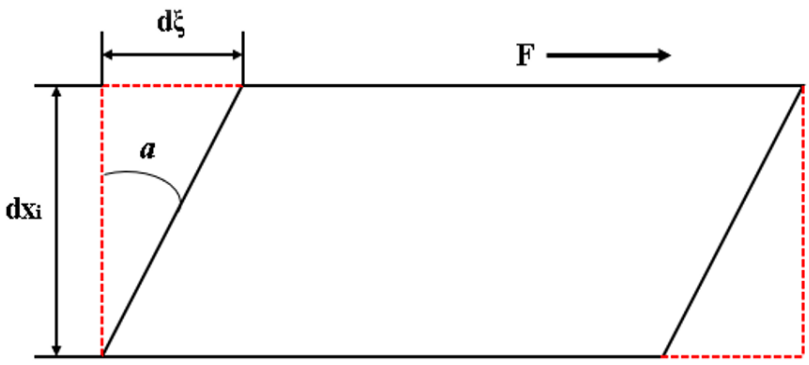

Figure I.2: Deformation of a fluid particle.

I.3 Dimensionless Numbers:

Dimensionless numbers in fluid mechanics constitute a set of quantities which play an important role in the analysis of fluid behavior. They reduce the number of variables describing a system, thereby reducing the number of data It is necessary to establish correlations of physical phenomena.

I.3.1 Reynolds number:

The Reynolds Re number represents the ratio of inertial and force viscous. This dimensionless number appears naturally by dimensioning the equations of Navier-Stokes. It is defined as follows:

$$Re = \frac{\rho d u}{\mu_p} \tag{I.6}$$

In the case of non-Newtonian fluids, it is necessary to use apparent viscosity. Because in the laminar flow in a pipe the shear stress varies according to of radial positions y and also viscosity.

In this case we use the generalized Reynolds number proposed by Metzner and Reed [6] defined by:

$$Re_{g,n} = \frac{\rho d^n u^{2-n}}{8^{n-1} K \left(\frac{3n+1}{4n} \right)^n} \tag{I.7}$$

I.3.2 Bingham Number:

The Bingham number, denoted as Bn, plays a crucial role in the analysis of viscoplastic fluid flows. It serves as a parameter that signifies the relationship between the effects of plasticity, specifically the stress effects associated with the threshold, and the viscous effects within the fluid. The Bingham number is instrumental in quantifying the balance between the material's resistance to flow (threshold stress) and its viscous behavior. This dimensionless number provides valuable insights into the viscoplastic characteristics of a fluid, aiding in the understanding and prediction of its flow behavior under different conditions.

$$Bn = \frac{\tau_y d}{\mu_p U} \tag{I.8}$$

I.3.3 Hedström number:

The Hedstrom number is a useful dimensionless parameter that often appears in non-Newtonian fluid studies, given by:

$$He = \frac{(\rho d^2)\tau_y}{\mu_p} \tag{I.9}$$

It serves to characterize the type of flow (laminar or turbulent) for fluids that follow the Bingham law.

I.4 Fluid classification:

I.4.1 Newtonian fluids:

Newtonian fluids, a concept introduced by Sir Isaac Newton, are characterized by a straight forward linear relationship between the deformation rate and applied shear stress. This fundamental behavior is not confined to theoretical discussions but finds practical application in everyday fluids like water, air, and oils, as highlighted in Figure I.3. The consistency in the connection between shear stress and deformation rate defines the predictable behavior of Newtonian fluids.

Conversely, the mechanical response of non-Newtonian fluids, exemplified by substances such as blood and liquid plastics, deviates from this linear correlation. The non-linear relationship between shear stress and deformation rate in these materials adds a layer of intricacy to their behavior [1]. This departure from Newtonian behavior holds significant implications across diverse fields, influencing areas from industrial processes to biomedical research. Recognizing and classifying fluids based on their rheological characteristics becomes pivotal for optimizing processes and understanding the complexities inherent in these fluid systems.

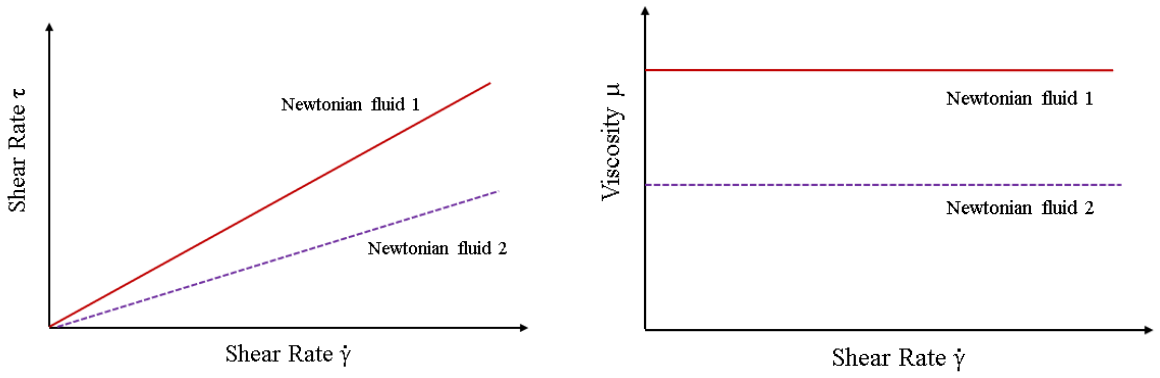

Figure I.3: Comparison of Newtonian Flow Behavior.

In a one-dimensional shear flow of Newtonian fluids, the shear stress is expressed by the linear relationship (see equation I.2).

I.4.2 Non-Newtonian Fluids:

A non-Newtonian fluid is distinguished by the variability of its viscosity, which is not constant and can depend on parameters associated with flow or time. A comprehensive understanding of these materials involves recognizing a range of behaviors that can be encountered when dealing with non-Newtonian fluids. Some of the notable behaviors include:

I.4.2.1 Fluids independent of time:

Non-Newtonian fluids independent of time are the fluids that obey the relationship:

$$\tau_{ij} = \mu(\dot{\gamma}_{ij})\dot{\gamma}_{ij} \tag{I.10}$$

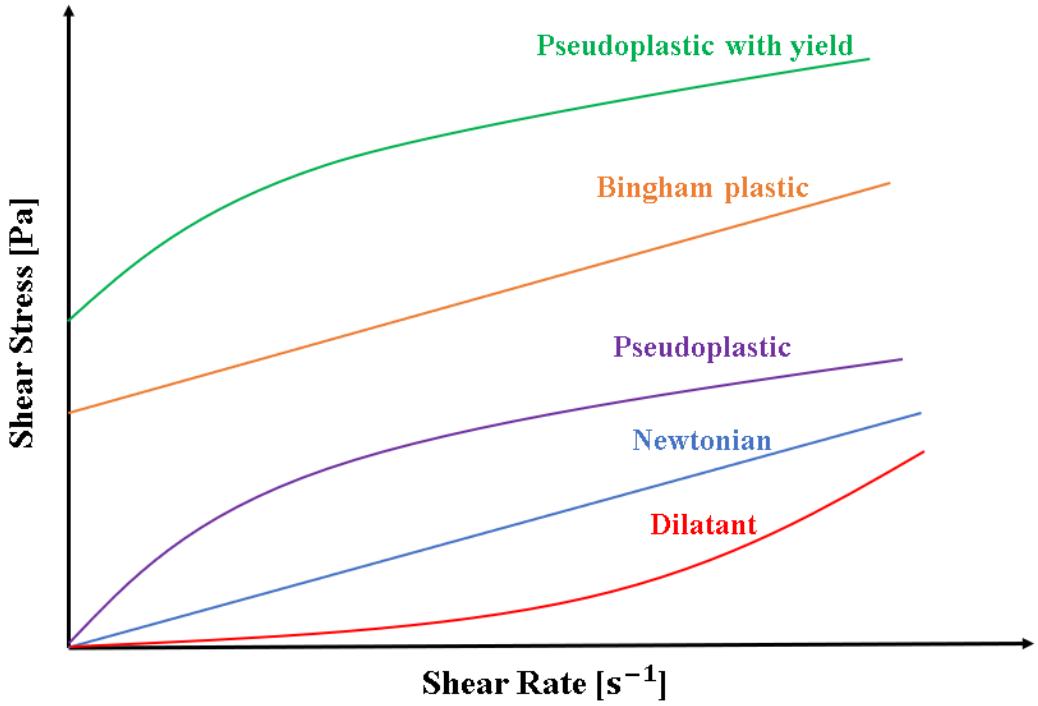

Figure I.4: Different rheological behaviors.

Where the viscosity (γ) depends on the rate of deformation, there are three types of fluids time independent:

a) The fluids (shear thinning):

The distinctive rheogram with a concavity turned down, as shown in Figure I.3, serves as a signature characteristic of these liquids. This unique behavior, where viscosity diminishes with increasing shear, is visually captured in Figure I.3 by the descending trend in apparent viscosity (μ app). Ostwald's power rule, recommended for modeling, provides a valuable framework applicable to several types of liquids exhibiting this intriguing rheological response. By incorporating this empirical relationship, our understanding of these fluids and their dynamic behavior is enhanced, laying the groundwork for further exploration and analysis in our study.

$$\tau_{ij} = K\dot{\gamma}^{n} \quad (I.11)$$

Where the behavior index $n < 1$.

b) The Dilating Fluids (Rheo-thickening Fluid):

These are fluids whose viscosity increases with the shear rate. The dilating fluid is much more rarely observed than pseudo-plastic. However, some suspensions concentrated (corn starch for example) and wet sand have a dilating behavior. Fluid can be pseudo-plastic for a certain range of shear rates, and dilators for another.

Among the time-independent fluids, this subclass received very little attention; by very little reliable data is available. Until recently, the behavior of expansion fluids was considered to be much less widespread in the chemical and treatment [7].

We use the law of power in equation (I.11), With an exponent n >1 which is the larger the material deviates from the behavior Newtonian.

c) Viscoplastic fluids:

This is a special case of non-Newtonian fluids, these fluids flow only from of a certain constraint, called threshold constraint τ_y. Below this, they behave as solids and beyond they flow as a Newtonian or shear thinning fluid. This property meets in some highly concentrated polymer solutions and suspensions, and in life common with toothpaste, yogurt, ketchup or clays (Lapointe and bentonite by example) and drilling sludge. This behavior can be interpreted by the presence of aggregates in the material or gels that remain up to the threshold stress. For suspension concentrated, a network of interactions can indeed exist and must be broken to cause suspension flow [8].

Several mathematical models exist to describe the rheological behavior of a threshold fluid. All of which are simply the fitting results of the empirical curves. The most used are:

- **Bingham Model:**

A fluid with a linear curve for, where τ_y is the threshold stress, $\tau_{ij} > \tau_y$ is called a Bingham plastic fluid. This type of fluid is distinguished by a constant plastic viscosity K, which represents the slope of the shear stress curve as a function of the shear rate. The presence of this plastic viscosity characterizes the particular behavior of Bingham plastic fluids, where a stress threshold must be reached before the fluid begins to flow significantly.

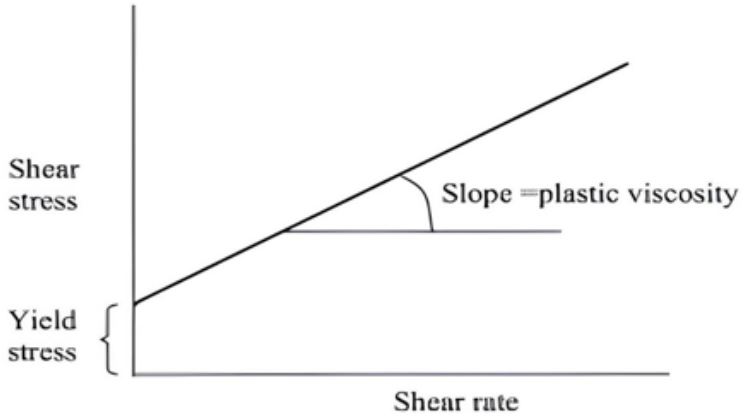

Figure I.5: Rheological behavior of Bingham fluid.

The equation describing the flow behavior of this fluid in constant shear at a single dimension is written:

$$\begin{cases} \tau_{ij} = \tau_y + \mu_p \dot{\gamma} & \text{for } \tau_{ij} > \tau_y \\ \dot{\gamma} = 0 & \text{for } \tau_{ij} \leq \tau_y \end{cases} \quad \text{(I.12)}$$

- **Herschel-Bulkley Model:**

It represents a straightforward extension of the Bingham fluid model to accommodate non-flow curves. This model is defined by three constants: the consistency K, the index of fluid structure n, and the threshold stress τ_y. These parameters collectively characterize the rheological behavior of the fluid, capturing its resistance to flow, structural properties, and the minimum stress required for significant deformation to occur.

$$\begin{cases} \tau_{ij} = \tau_y + K\,\dot{\gamma}^n & \text{for } \tau_{ij} > \tau_y \\ \dot{\gamma} = 0 & \text{for } \tau_{ij} \leq \tau_y \end{cases} \quad \text{(I.13)}$$

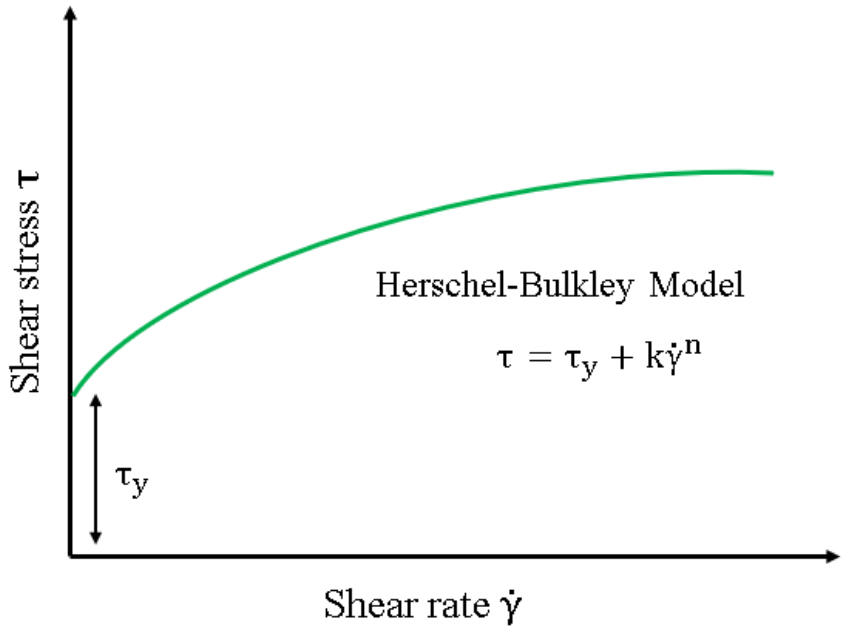

Figure I.6: Herschel-Bulkley fluid behavior.

The apparent viscosity is therefore:

$$\begin{cases} \eta = K\dot{\gamma}^{n-1} + \dfrac{\tau_y}{\dot{\gamma}} & \text{for } \tau_{ij} > \tau_y \\ \eta \to \infty & \text{for } \tau_{ij} > \tau_y \end{cases} \tag{I.14}$$

- **Casson Model:**

The Casson model, recognized for its effectiveness in simulating blood flow, holds particular relevance in studying fluid dynamics within narrow arteries. The work by Merrill et al [9] has underscored the model's utility by demonstrating its satisfactory prediction of blood flow patterns in blood tubes with diameters spanning 130 to 1000 µm. This highlights the Casson model's capacity to capture the nuanced rheological intricacies inherent in the flow of blood through vessels of varying sizes, providing valuable insights for biomedical applications and furthering our understanding of hemodynamics in physiological contexts.

The model is defined by the relationship:

$$\begin{cases} \sqrt{\tau_{ij}} = \sqrt{\tau_y} + K\dot{\gamma} & \text{for } \tau_{ij} > \tau_y \\ \dot{\gamma} = 0 & \text{for } \tau_{ij} \le \tau_y \end{cases} \tag{I.15}$$

I.4.2.2 The fluids depend on time:

There are two categories of time-dependent non-Newtonian fluids: those with a constant shear speed but varying viscosity with time. Thixotropic is one type and rheopectic is the other.

a) Thixotropic fluids:

Thixotropic fluids have a viscosity that decreases with time when a stress is applied to them. By definition thixotropy is a reversible variation in viscosity when a fluid is subjected to stress. This assumes that as soon as the stress applied is stopped, the viscosity of the material increases again until reaching its original value at the end of this behavior is interpreted as changes in the internal structure of the and even a gradual destruction of this microstructure. This can be spatial configuration of particles for suspensions or droplets for emulsions, or still intertwining macromolecules for polymers. The modification then results in competition between hydrodynamic forces (which destroy the microstructure) and cohesion and Brownian movement (which reform the microstructure) [10].

b) Anti-thixotropy fluids:

Less commonly observed than thixotropy, we encounter a contrasting behavior known as anti-thixotropy, or rheopexy [10].In this phenomenon, the apparent viscosity of the material increases over time in response to a given strain or strain rate. This rheological characteristic represents a departure from the more prevalent thixotropic behavior, demonstrating the diverse and intricate range of fluid responses that can be encountered in specific materials under varying conditions.

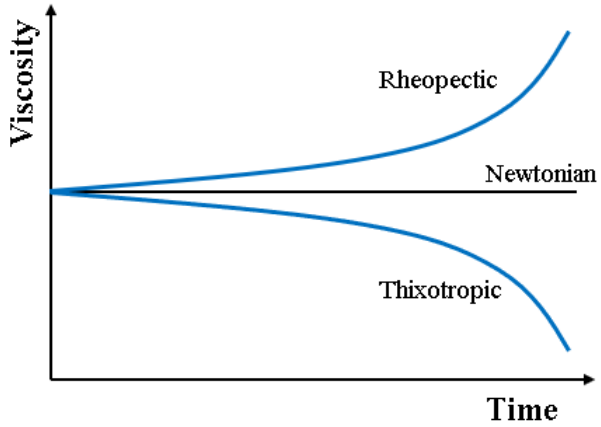

Figure I.7: Rheological behavior of time-dependent fluids.

I.5 Previous work:

Evan Mitsoulis and R.R. Huilgol [11] conducted a comprehensive quantitative analysis of entry flows through abrupt expansions for Bingham plastics exhibiting yield stress. They utilized Papanastasiou's modification of the Bingham constitutive equation, applying it across the flow field in both yielded and unyielded regions. The study focused on determining the vortex shape, size, and intensity, as well as the extent of yielded/unyielded zones for planar and axisymmetric expansions across a range of Reynolds ($0 \leq Re \leq 200$) and Bingham numbers ($0 \leq Bn < \infty$). Pressure measurements were used to identify excess pressure losses, leading to an input correction equation. This research enhances understanding of viscoplastic fluid behavior under varying conditions.

The research of Khaled J. Hammad with G. C. Vradis and M. V. Ötügen [12] investigates the behavior of Herschel-Bulkley fluids, which have yield stress and shear-thinning/thickening properties, in sudden pipe expansions using numerical simulations. Common in food processing, paints, and drilling slurries, these fluids' steady, laminar flow was analyzed under varying conditions: Reynolds number (50 to 200), yield number (0 to 2), and power-law index (0.6 to 1.2). Findings reveal two flow regimes: recirculating flow at high flow rates and low yield stress, and stagnant zones at low flow rates and high yield stress. Yield stress significantly influences flow, with shear-thinning/thickening effects more prominent at lower yield stress, providing valuable insights for engineers designing piping systems for non-Newtonian fluids.

G. C. Vradis and M. V. Ötügen investigated the flow of viscoplastic Bingham fluids through sudden axisymmetric widening, employing numerical solutions for elliptic continuity equations. Their study explored various Reynolds numbers and threshold stress values, revealing laminar flow conditions with constant fluid properties. Their findings offer crucial insights into how such fluids behave in sudden axisymmetric widening scenarios, highlighting the complex interactions of key parameters. Additionally, they demonstrated the applicability of the finite-difference technique in analyzing separating and reattaching internal flows of Bingham plastics [13].

Other studies made by Khaled J. Hammad [14], a combined experimental and computational study investigated the laminar flow of a nonlinear viscoplastic fluid through an axisymmetric sudden expansion. The study covered a range of Reynolds numbers, revealing two distinct flow regimes characterized by the presence or absence of a recirculating flow zone downstream of the expansion step. Lastly, in [15] , Khaled J. Hammad investigated the flow of viscoplastic

non-Newtonian fluids through axisymmetric sudden expansions. Their study revealed two distinct viscoplastic flow regimes dependent on Reynolds and yield numbers, transitioning from recirculating to non-recirculating flow regimes with increasing yield numbers.

Both Bekhadra's [16] study and Hegaj's [17] paper investigate non-Newtonian fluid flow through sudden expansions using the Herschel-Bulkley model. They analyze the influence of Reynolds number, Bingham number, and power-law index on flow characteristics. Numerical simulations are utilized to examine velocity, pressure fields, and flow structure, discussing the impact of these parameters on the fluid behavior, including recirculation zone length and dead zone distribution. Bekhadra's study focuses on laminar flow through an axisymmetric expansion, varying Re, Bn, and n, with ANSYS-Fluent simulations highlighting effects of plasticity and inertial forces. It provides numerical correlations for circulation zone length and observes Bn's influence on local loss coefficient. Hegaj's paper explores a wider parameter range, presenting fluid flow characteristics and their effect on dead zone distribution in a planar channel expansion.

In other article of Bekhadra [18], [19]. numerical study on laminar Bingham fluid flow through an axisymmetric sudden expansion, the focus is on varying aspect ratios and Reynolds numbers and Bingham Number [0-2]. ANSYS-Fluent is again employed to analyze Bingham flow, determining recirculation zone length and intensity and shedding light on the local loss coefficient. Results show increased reattachment length and eddy intensity with increasing Reynolds number and aspect ratio, while decreasing with higher Bingham numbers. The local loss coefficient increases with aspect ratio for both Newtonian and Bingham fluids, and increasing Bingham number also raises it. Dimensionless equations are developed to predict reattachment lengths, eddy intensity, and local loss coefficient.

Flávia Zinani's paper [20] introduces Galerkin Least-Squares (GLS) methods for Bingham plastic fluid flows using the Generalized Newtonian Liquid (GNL) model with Papanastasiou’s regularization. It combines conservation equations of mass and momentum with the GNL constitutive equation, overcoming typical Galerkin challenges. Numerical simulations include lid-driven cavity flows for validation, as well as shear-thinning fluids without yield stress limits and Bingham plastic creeping flows through expansions. Results reveal distinct unyielded regions, aiding in understanding Bingham fluid behavior in expansion flows.

This study of Sergio L. D. Kfuri [21] investigates friction coefficients for non-Newtonian fluids in pipeline systems, crucial for efficient design. Comparisons are made between

Newtonian fluids and two categories: pseudoplastic fluids modeled as power-law and yield stress fluids modeled as Bingham. Poly flow is utilized to compute friction losses in laminar flow through abrupt contractions and expansions. Aspect ratio notably affects local friction coefficients in expansions more than contractions. The power index (n) similarly influences both cases. Dilatant fluids exhibit the lowest friction coefficient (K) at low Reynolds numbers, with a reversal at higher Reynolds numbers. The effect of yield stress (s0 y) differs between contractions and expansions. Equations are proposed for each accessory, accounting for fluid rheological parameters and Reynolds number, with satisfactory precision for engineering applications.

The research by A. Manouer [22] delves into the numerical exploration of the laminar flow of a non-Newtonian fluid (exhibiting shear-thinning behavior) passing through a 1:3 planar gradual expansion. Various combinations of Power-Law indices (0.6, 0.8, and 1.0), expansion angles (15°, 30°, 45°, 60°, and 90°), and different generalized Reynolds numbers ($1 \leq Re\ g \leq 400$) are investigated. Analysis of these parameters' influence on flow patterns facilitates the identification of two critical generalized Reynolds numbers (Re gcr1 and Re gcr2). These critical values mark the transition from symmetric to asymmetric flow and the emergence of a third recirculation zone, respectively. The findings reveal that reducing either the Power-Law index or the expansion angle enhances flow stability, notably elevating the two critical generalized Reynolds numbers. To predict these critical values, two correlations are proposed.

Numerical investigation using the finite-volume approach has been conducted to study the laminar flow of a Newtonian fluid in an axisymmetric pipe expansion by P. J. Oliveira [23]. The study compared predicted overall flow characteristics, such as recirculation length, strength, and center location, with experimental data and correlations, showing good agreement. The aim was to assess the pressure-loss coefficient C across a range of Reynolds numbers and compare the findings with existing simplified theory based on a one-dimensional (1-D) overall balance of energy and momentum. Significant disparities were identified, prompting the formulation of corrected theoretical equations within the scope of the 1-D approximation. These corrections, derived from numerical results, addressed three factors: (1) differences between actual and fully developed wall friction, (2) distortion of velocity profiles from the parabolic shape at the sudden expansion section, and (3) nonuniformity of pressure at the expansion plane. Predicted loss coefficient values showed agreement within 4% with the corrected theory and exhibited proportionality to the inverse of the Reynolds number for $Re \leq 17.5$, with effect (3) being predominant and accounting for up to 85% of C, and approximately constant for Re >

17.5, where effect (1) was predominant and accounted for 20% of C. Lastly, a correlation is proposed for calculating the local loss coefficient as a function of the Reynolds number for the 1:2.6 sudden expansion under fully developed conditions.

I.6 Conclusion:

In conclusion, this chapter provides a comprehensive examination of fluid flow Newtonian and non-Newtonian and their modeling, also synthesizing previous research and give an overview of them. The theoretical framework utilized for analyzing these flows is meticulously detailed, forming the foundation for our work. Our research specifically addresses the prediction of fluid behavior in non-standard scenarios using advanced computational models, contributing significant insights to the field.

Chapter II

The Physical Model and Mathematical Framework

Introduction:

In this study, we delve into the investigation of fluid dynamics, specifically focusing on flows characterized by permanence and laminarity. The fluid under examination is an incompressible non-Newtonian fluid navigating through a sudden expansion. The governing principles of these fluid dynamics are encapsulated by the continuity equations and momentum conservation equations, derived from the esteemed Navier-Stokes framework. These equations serve as the cornerstone for understanding the intricate interplay between mass conservation and momentum changes within the fluid as it undergoes the transformative process of a sudden expansion.

Our exploration aims to unravel the nuanced behaviors and phenomena inherent in these flows, shedding light on the underlying dynamics that shape their trajectory through the sudden expansion.

II.1 Problem description:

II.1.1 Geometry:

The geometry studied herein is an axisymmetric depicted in Figure II.1, the inlet section of the small channel has radius R_1 and the outlet section has radius R_2, ratios were considered 1:2. The length of the small channel L_1 is fixed as twenty-five times its diameter, while the length of the large channel L_2 is seventy-five times.

A parabolic velocity profile in the horizontal direction is established at the inlet of the flow, while free traction at is maintained the flow outlet.

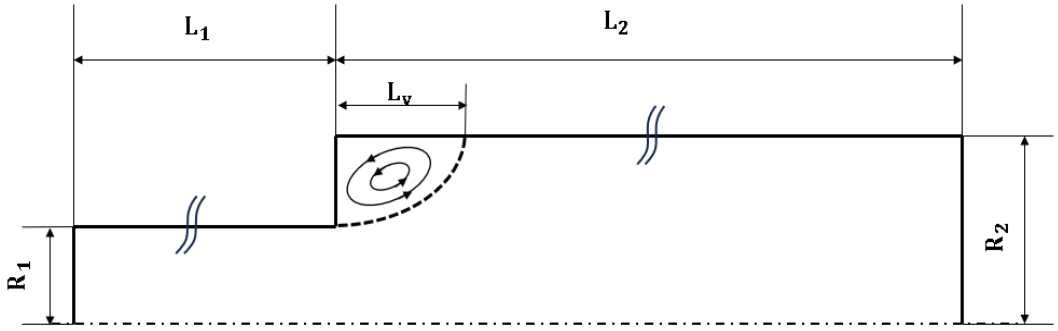

Figure II.1: Depiction the geometric of the study.

II.1.2 Rheological parameters of the fluid:

Our study focuses on two models of fluid, the first one acts like thick liquid (Bingham fluid) with a constant viscosity of $\mu_p = 0.1075 Pa.s^n$. the second is Hershel-Bulkley model behavers similarly, its consistence is enumerated as $K = 0.283 Pa.s^n$ with different index $n = [0.6;\ 0.8 \text{ and } 1.8]$.

Notably, the density registers at $\rho = 807.8\ kg/m^3$.

II.2 Government equations:

II.2.1 The conservation of mass:

In classical mechanics, mass conservation holds, and in continuum mechanics, this principle is applied, stating that the mass of a continuous medium remains constant. The continuity equation can be extended to cylindrical coordinates (x, r, θ) and corresponding velocities $(u_x,\ u_r,\ u_\theta)$ [24], [25].

$$\frac{\partial(u_x)}{\partial x} + \frac{1}{r}\frac{\partial(r u_r)}{\partial r} + \frac{1}{r}\frac{\partial(u_\theta)}{\partial \theta} = 0 \tag{II.1}$$

II.2.2 The conservation of momentum:

Coordinate system (ox):

$$\rho\left(\frac{\partial u_x}{\partial t} + u_x\frac{\partial u_x}{\partial x} + u_r\frac{\partial u_x}{\partial r} + \frac{u_\theta}{r}\frac{\partial u_x}{\partial \theta}\right) = -\frac{\partial p}{\partial x} + \left(\frac{\partial \tau_{xx}}{\partial x} + \frac{1}{r}\frac{\partial}{\partial r}(r\tau_{rx}) + \frac{1}{r}\frac{\partial \tau_{\theta x}}{\partial \theta}\right) \tag{II.2}$$

Coordinate system (or):

$$\rho\left(\frac{\partial u_r}{\partial t} + u_x\frac{\partial u_r}{\partial x} + u_r\frac{\partial u_r}{\partial r} + \frac{u_\theta}{r}\frac{\partial u_r}{\partial \theta} + \frac{{u_\theta}^2}{r}\right) = -\frac{\partial p}{\partial r} + \left(\frac{\partial \tau_{xr}}{\partial x} + \frac{1}{r}\frac{\partial}{\partial r}(r\tau_{rr}) + \frac{1}{r}\frac{\partial}{\partial \theta}(\tau_{\theta r}) - \frac{\tau_{\theta\theta}}{r}\right) \tag{II.3}$$

Coordinate system $(o\theta)$:

$$\rho\left(\frac{\partial u_\theta}{\partial t} + u_x\frac{\partial u_\theta}{\partial x} + u_r\frac{\partial u_\theta}{\partial r} + \frac{u_\theta}{r}\frac{\partial u_\theta}{\partial \theta} + \frac{u_r u_\theta}{r}\right) = -\frac{1}{r}\frac{\partial p}{\partial \theta} + \left(\frac{\partial \tau_{x\theta}}{\partial z} + \frac{1}{r^2}\frac{\partial}{\partial r}\left(r^2\tau_{r\theta}\right) + \frac{1}{r}\frac{\partial \tau_{\theta\theta}}{\partial \theta} + \frac{\tau_{\theta r} - \tau_{r\theta}}{r}\right) \tag{II.4}$$

For a generalized Newtonian model, the stress tensor

$$\tau_{ij} = 2\eta(\dot{\gamma})D_{ij} \tag{II.5}$$

While the η viscosity, D_{ij} the rate of deformation tensor expressed by:

$$D_{ij} = \frac{1}{2}\left(\frac{\partial u_i}{\partial x_j} + \frac{\partial u_j}{\partial x_i}\right) \tag{II.6}$$

and $\dot{\gamma}$ is the rate of deformation intensity defined as a second invariant of D_{ij}:

$$\gamma = \sqrt{2D_{ij} : D_{ij}} = \sqrt{2\left[\left(\frac{\partial u_r}{\partial r}\right)^2 + \left(\frac{u_r}{r}\right)^2 + \left(\frac{\partial u_x}{\partial x}\right)^2\right] + \left[\frac{\partial u_r}{\partial x} + \frac{\partial u_x}{\partial r}\right]^2} \tag{II.7}$$

As a result, the nondimensional effective viscosity is defined as:

$$\tau_{ij} = \left[k\left(\frac{1}{2}D_{ij}D_{ij}\right)^{(n-1)/2} + \frac{\tau_y}{\left(\frac{1}{2}D_{ij}D_{ij}\right)^{1/2}}\right]D_{ij} \text{ for: } \frac{1}{2}\tau_{ij}\tau_{ij} \le {\tau_y}^2 \tag{II.8}$$

$$D_{ij} = 0 \text{ for: } \frac{1}{2}\tau_{ij}\tau_{ij} \le {\tau_y}^2 \tag{II.9}$$

II.2.3 Simplification:

Our study is about the flow displays an 2D axisymmetric model and the fluid conforms to the Bingham model.

So, the simplification becomes:

$$\frac{\partial u_x}{\partial x} + \frac{1}{r}\frac{\partial u_r}{\partial r} = 0 \tag{II.10}$$

$$\rho\left(u_x\frac{\partial u_x}{\partial x} + u_r\frac{\partial u_r}{\partial r}\right) = -\frac{\partial p}{\partial x} + \left(\frac{\partial \tau_{xx}}{\partial x} + \frac{1}{r}\frac{\partial}{\partial r}(r\tau_{rx})\right) \tag{II.11}$$

$$\rho\left(u_x\frac{\partial u_r}{\partial x} + u_r\frac{\partial u_r}{\partial r}\right) = -\frac{\partial p}{\partial r} + \left(\frac{\partial \tau_{rx}}{\partial x} + \frac{1}{r}\frac{\partial}{\partial r}(r\tau_{rr})\right) \tag{II.12}$$

II.3 Boundary conditions:

In the analyzed domain, the imposed boundary conditions are:

_ Inlet:

At the inlet, a fully developed velocity profile of a viscoplastic fluid:

$$u_x \neq 0, u_r = 0 \tag{II.13}$$

_ Wall:

we prescribe the no-slip condition, which means the velocity of the fluid at the solid boundary is forced to be zero as it expressed at the equation bellow:

$$u_x = 0, u_r = 0 \tag{II.14}$$

_ Axe:

On the axe, symmetry condition is applied:

$$\frac{\partial u_x}{\partial r} = u_r = 0 \; ; \; \frac{\partial p}{\partial r} = 0 \tag{II.15}$$

_ Outlet:

At the outlet, a constant pressure condition is imposed, corresponding to atmospheric pressure:

$$\frac{\partial u_x}{\partial x} = \frac{\partial u_r}{\partial x} = 0 \; ; \; p = 0 \tag{II.16}$$

II.4 Velocity profile:

in the context of fluid mechanics, the velocity profile refers to the variation of the flow speed (velocity) across a flowing channel's cross-section. It essentially depicts how fast the fluid particles are moving at different positions within that cylindrical pipe. Interestingly, Bingham plastic fluids exhibit a unique velocity profile characteristic when in laminar flow, a distinction not observed in other fluids.

A flow can function as a displacement fluid by pushing it in front of it due to its yield stress. In an application like this, it's important to forecast where in the fluid the material will flow when the stress exceeds the yield stress and where it will remain motionless or move as a solid plug when the stress is too low.

The diagram indicates the geometry of the channel under consideration (Figure II.2) following the coordinate (r; θ), which shows iso-velocity zone in the center of the flow, ant this represent the non-sheared area and a velocity gradient zone in the vicinity of the wall which also represent the sheared area.

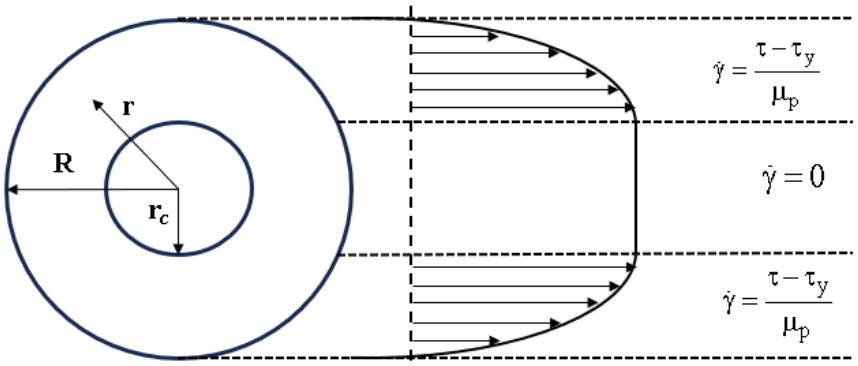

Figure II.2: Velocity profile for the flow of Bingham fluid in a cylindrical pipe in laminar mode [26].

r_c is the critical radius that separates the two zones.

Based on our study, the distribution of the linear shear stresses on the cross-section of the pipe is as follows:

$$\tau(r) = \frac{r}{2}\frac{\Delta P}{L} \tag{II.15}$$

$$\tau_w = \frac{R}{2}\frac{\Delta P}{L} \tag{II.16}$$

Constitutive equation:

$$\tau - \tau_y = \frac{\tau_w}{R}(r - r_c) = \pm\mu_B\dot{\gamma} = \pm\mu_B\frac{\partial u}{\partial r} \tag{II.17}$$

When we relate that to our deformation field we end up with an integral:

$$\int_{r}^{R} \frac{\tau_w}{R}(r - r_c)\, dr = -\int_{v}^{0} \mu_B\, du \tag{II.18}$$

After integrate the equation (II.18). We got:

$$u(r) = \frac{\tau_w}{R\mu_B}\left(\frac{R^2 - r^2}{2} - r_c(R - r)\right) \tag{II.19}$$

The equation (II.19) is only available for $r > r_c$.

in case of $r \leq r_c$, it becomes:

$$u(r) = \frac{\tau_w}{2R\mu_B}\left[R^2 - {r_c}^2\right] - \frac{\tau_w r_c}{R}\left(R - r_c\right) \tag{II.20}$$

II.5 Notion of head loss:

In fluid mechanics, head loss or what also called pressure loss refers to the energy wasted by a flowing fluid due to friction and turbulence. This energy loss shows up as a pressure drop along the flow path.

There are two main types of head loss:

II.5.1 Major head loss:

Represent the head losses caused by friction in pipes due to the fluid's viscosity. These losses can be calculated using the following formula:

$$\Delta p_L = \frac{\lambda}{2d}\rho U_i^2 \tag{II.21}$$

II.5.2 Minor head loss:

These losses are caused by changes in the flow path, such as cones, or the changing of the radius like an expansion. It can still be significant as [27]:

$$\Delta p_S = k\frac{\rho U_i^2}{2} \tag{II.22}$$

II.6 Conclusion:

In conclusion, this chapter has provided a detailed exploration of the considered problem, presenting a comprehensive description and the governing equations for the flow of a non-Newtonian fluid through a sudden expansion, with applied boundary conditions. The meticulous examination of the physical model and mathematical framework lays a solid foundation for the subsequent chapters.

In addition, we presented our findings on the velocity profile and the Bingham fluid's behavior within the pipe under study.

The insights gained from this chapter not only enhance our understanding of the non-Newtonian fluid dynamics problem at hand but also pave the way for a systematic and rigorous exploration in the chapters to come.

Chapter III

Numerical Methods

Introduction:

Our research employs numerical simulations with ANSYS Fluent, a finite volume method-based software, known for its advantages in modeling fluid flow. Emphasizing the pivotal role of numerical methods in resolving Navier-Stokes equations, we highlight their ability to provide approximate solutions while controlling errors. Fluid dynamics, governed by essential equations like conservation of mass, momentum, and energy, present analytical challenges, prompting the use of Computational Fluid Dynamics (CFD) to transform continuous partial differential equations into a discrete system.

The transition from an exact to an approximated problem involves various techniques, such as Finite Difference, Finite Element, and Finite Volume methods, each competing and complementing one another. In upcoming sections, we delve into the intricate details of our numerical methodology. Additionally, we introduce ANSYS Fluent, that allows us to comprehensively model fluid dynamics, providing insights into the complexities of flow governed by fundamental conservation equations.

III.1 Principle of numerical computation:

The principle of numerical calculation is schematized as follows [28]:

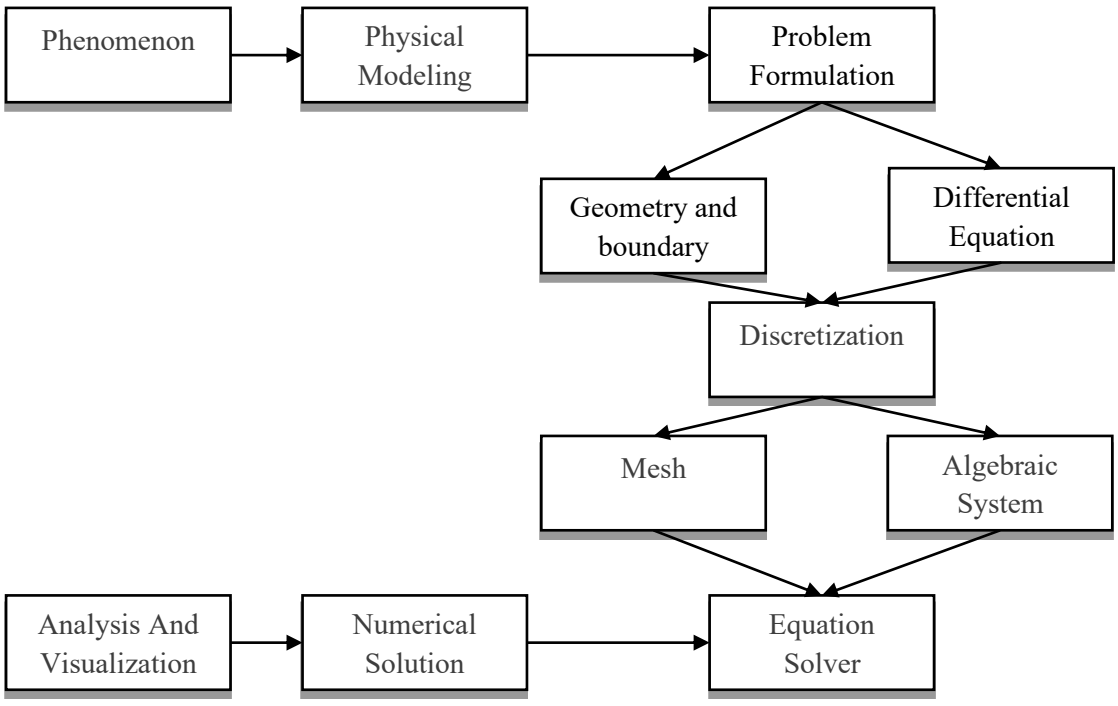

Figure III.1: Principle of numerical calculation.

III.2 The finite volume method (FVM):

The Finite Volume Method (FVM) was introduced into the field of computational fluid dynamics in the early seventies as outlined by McDonald in 1971 and MacCormack and Paullay in 1972. Physically, the finite volume method (FVM) relies on maintaining a balance of fluxes across control volumes. And numerically, the finite volume method (FVM) extends finite difference methods (FDM) in a geometric and topological context. In other words, finite volume schemes can be reduced to finite difference schemes [29].

The Finite Volume Method (FVM) stands as a discretization approach employed in the approximation of either a singular or a networked set of partial differential equations (PDEs) that articulate the conservation or equilibrium of one or more quantities. These PDEs, often denoted as conservation laws, exhibit diverse characteristics—be they elliptic, parabolic, or hyperbolic—and serve as foundational models across an extensive spectrum of disciplines, including physics, biophysics, chemistry, image processing, finance, and dynamic reliability. They delineate intricate relationships between the partial derivatives of unknown fields, such as temperature, concentration, pressure, molar fraction, density of electrons, or probability density function, concerning variables within the specified domain (space, time, etc.) [30].

The finite volume method is characterized by significant attributes, notably the local conservativity of numerical fluxes. This means that the numerical flux is conserved between discretization cells and their neighbors. This particular feature enhances the appeal of the finite volume method, especially in studies where the flux holds significance, as observed in fluid mechanics, heat transfer, and mass transfer problems [30].

III.3 Discretization in FVM:

The computational domain is divided into a series of subdomains called control volumes. These control volumes cover the entire computational domain without overlapping, such that the sum of their volumes is exactly equal to the volume of the computational domain. A point is positioned at the center of each volume and is called the center of the control volume, denoted as P The nodes of neighboring volumes are labeled according to their positions: N, S, W, E, T, and B (corresponding to the directions North, South, West, East, Top, and Bottom, respectively). (Figure III. 2).

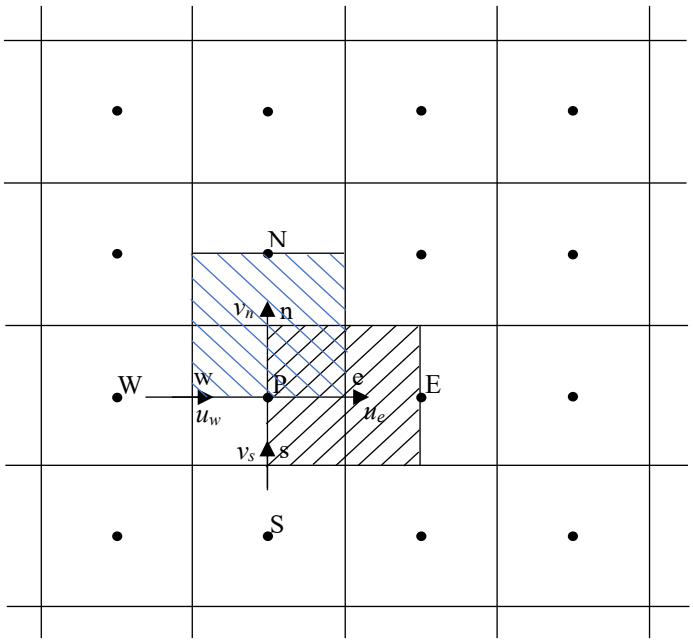

Figure III.2: Control volume distribution in an offset mesh [31].

In the finite volume method, the laws of conservation (mass, momentum, and energy) are expressed locally in integral form. The cornerstone of this method lies in Gauss's theorem (also known as the divergence theorem or Ostrogradski's theorem), which allows the transformation of a volume integral into a surface integral. The purpose of this method is to convert the general differential equation into a system of algebraic equations by relating the values of the considered variable to the adjacent nodal points of a typical control volume. This is achieved by integrating the governing differential equation within this control volume with the approximation of different terms (convection, diffusion, and source).

III.3.1 Discretization of the transport equation:

The transport equation for a scalar quantity, expressed in its integral form, in a steady-state regime is given by:

$$\int\left[\frac{\partial}{\partial x}(\rho u\varphi)+\frac{1}{r}\frac{\partial}{\partial r}(r\rho v\varphi)\right]dV=\int\left[\frac{\partial}{\partial x}\left(\Gamma\frac{\partial\varphi}{\partial x}\right)+\frac{1}{r}\frac{\partial}{\partial r}\left(r\Gamma\frac{\partial\varphi}{\partial r}\right)\right]dV+\int S_{\varphi}dV \qquad \text{(III.1)}$$

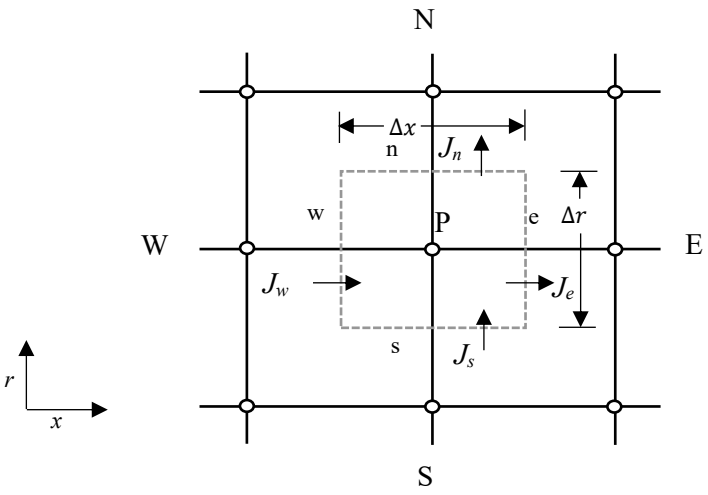

Figure III.3: A control volume for the case of an axisymmetric flow[31].

The integration of equation (III.1) over the control volume depicted in Figure (III.3), shows as:

$$J_e - J_w + J_n - J_s = \iint_V S_\varphi dV \tag{III.2}$$

Here, the subscripts e, w, n, and s denote evaluations at the east, west, north, and south faces of the respective control volume. The quantities J_e, J_w, J_n, and J_s represent integrated total fluxes (combining convection and diffusion) across the control volume faces and are expressed by the following equations.

$$\begin{aligned} J_e &= \int_s^n \left(\rho u\varphi - \Gamma \frac{\partial \varphi}{\partial x} \right)_e dr \\ J_w &= \int_s^n \left(\rho u\varphi - \Gamma \frac{\partial \varphi}{\partial x} \right)_w dr \\ J_n &= \int_s^n \left(\rho u\varphi - \Gamma \frac{\partial \varphi}{\partial x} \right)_n dx \\ J_s &= \int_s^n \left(\rho u\varphi - \Gamma \frac{\partial \varphi}{\partial x} \right)_s dx \end{aligned} \tag{III.3}$$

The value at a node is affected by its neighboring nodes, positioned at the center of each control volume.

$$
\begin{aligned}
J_e &= \left[\rho u_e \varphi_e - \frac{\Gamma_e}{\Delta x_{(EP)}} \left(\varphi_E - \varphi_P \right) \right] \Delta r \\
J_w &= \left[\rho u_w \varphi_w - \frac{\Gamma_w}{\Delta x_{(PW)}} \left(\varphi_P - \varphi_W \right) \right] \Delta r \\
J_n &= \left[\rho v_n \varphi_n - \frac{\Gamma_n}{\Delta x_{(NP)}} \left(\varphi_N - \varphi_P \right) \right] \Delta x \\
J_s &= \left[\rho v_s \varphi_s - \frac{\Gamma_s}{\Delta x_{(PS)}} \left(\varphi_P - \varphi_S \right) \right] \Delta x
\end{aligned}
\tag{III.4}
$$

The integration of the source term is obtained by assuming that S_ϕ is uniform on the control volume. then, it is written:

$$\iint_v S dV = S_U + S_P \varphi_P \tag{III.5}$$

As:

S_U: Source related to boundary conditions;

S_P: Source estimated at node P of the control volume under consideration.

Similarly, the integration of the continuity equation on the control volume of the figure (III.3) leads to:

$$F_e - F_w + F_n - F_s = 0 \tag{III.6}$$

When it's known as flow of faces according to flow direction, and it defined by:

$$
\begin{aligned}
F_e &= \rho u_e \Delta r \\
F_w &= \rho u_w \Delta r \\
F_n &= \rho v_n \Delta x \\
F_s &= \rho v_s \Delta x
\end{aligned}
\tag{III.7}
$$

D stands for dissemination:

$$\begin{aligned} D_e &= \frac{\Gamma}{\Delta x}\Delta r \\ D_w &= \frac{\Gamma}{\Delta x}\Delta r \\ D_n &= \frac{\Gamma}{\Delta r}\Delta x \\ D_s &= \frac{\Gamma}{\Delta r}\Delta x \end{aligned} \tag{III.8}$$

So, all discretized equation leads to:

$$a_P\varphi_P = a_E\varphi_E + a_W\varphi_W + a_N\varphi_N + a_S\varphi_S + b \tag{III.9}$$

The order of this equation can be as follows:

$$a_P\varphi_P = \sum_{i=N,S,E,W} a_i\varphi_i + b \tag{III.10}$$

So that:

$$\begin{aligned} a_E &= D_e A(|P_e|) + -F_e, 0 \\ a_W &= D_w A(|P_w|) + F_w, 0 \\ a_N &= D_n A(|P_n|) + -F_n, 0 \\ a_S &= D_s A(|P_s|) + -F_s, 0 \\ a_P &= a_E + a_W + a_N + a_S + S_P \\ b &= S_U \end{aligned} \tag{III.12}$$

as known, that:

$$P_i = \frac{F_i}{D_i} \tag{III.13}$$

III.4 Notion of mesh:

In numerical modeling, conservation equations are reformulated on elementary volumes called elements or meshes. The discrete equations are solved at specific points known as discretization nodes, which are associated with these elements. The placement of these nodes can vary, occurring at the vertices, center, or faces of the elements, contingent upon the chosen discretization technique [32].

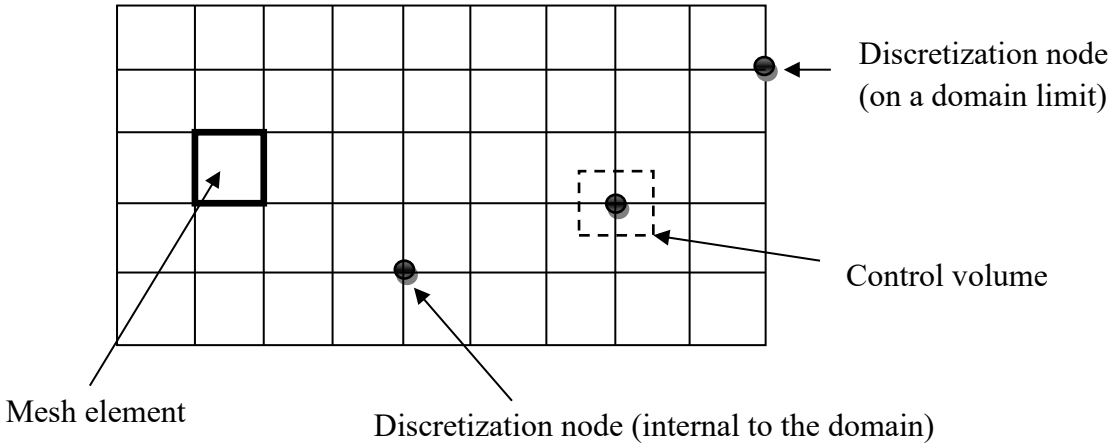

Figure III.4: Illustration of the mesh design.

III.5 Presentation of calculation code:

There are a number of industrial codes, with the best performances, allowing the prediction of fluid flows such as (FLUENT, CFX, PHOENICS, STAR-CD, TRIO, FEMLAB, CFD-ACE, FLOTRAN, N3S, CFDS-FLOW3D …) [31].

Computational Fluid Dynamics (CFD) has become an essential tool in engineering and scientific research for predicting fluid flows and understanding complex physical phenomena. Various industrial codes have been developed to simulate and analyze fluid dynamics [30], with each offering unique features and capabilities. Among these, ANSYS FLUENT stands out as a powerful software solution developed by the ANSYS group.

ANSYS FLUENT is widely utilized for modeling fluid flow, heat transfer, mass transfer, chemical reactions, and other aspects of computational fluid dynamics. It is capable of handling both compressible and incompressible fluids, making it versatile for a wide range of applications. The software is particularly adept at addressing complex physical phenomena such as turbulence, thermal transfer, and chemical reactions, making it an invaluable tool for engineers and researchers working on diverse projects.

One notable feature of ANSYS FLUENT is its streamlined CFD process, which can be executed within a single window. This efficiency is facilitated by a modern and user-friendly interface, allowing users to navigate through the software seamlessly. The interface aids in setting up simulations, defining parameters, and visualizing results, contributing to a more straightforward and accessible CFD experience.

The capabilities of ANSYS FLUENT make it suitable for applications in various industries, including aerospace, automotive, energy, and environmental engineering. Its ability to provide accurate predictions and insights into fluid behavior under different conditions makes it a go to choose for professionals seeking robust simulations.

The simulation process in ANSYS FLUENT typically involves three main stages: Preprocessing, Solving, and Postprocessing.

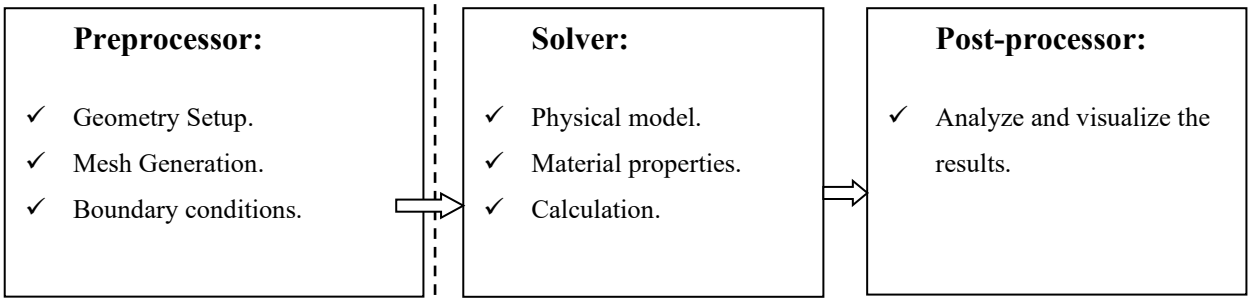

Figure III.5: Basic structure of the calculation code -ANSYS Fluent -[32].

III.5.1 Solver settings: Choosing a Solver:

A crucial part of setting up a FLUENT simulation is choosing the right solver. The solver settings determine how FLUENT calculates the governing equations that represent the physics of our problem.

There are two kinds of solvers available in FLUENT:

_Pressure-Based Solvers.

_Density-Based Coupled Solver (DBCS).

The figure (III. 6) below shows a flowchart of a process for solving transport equations.

The specific transport equations that need to be solved will depend on the type of fluid flow problem being modeled. However, the general steps outlined in the flowchart are typically followed for all types of transport equation solvers.

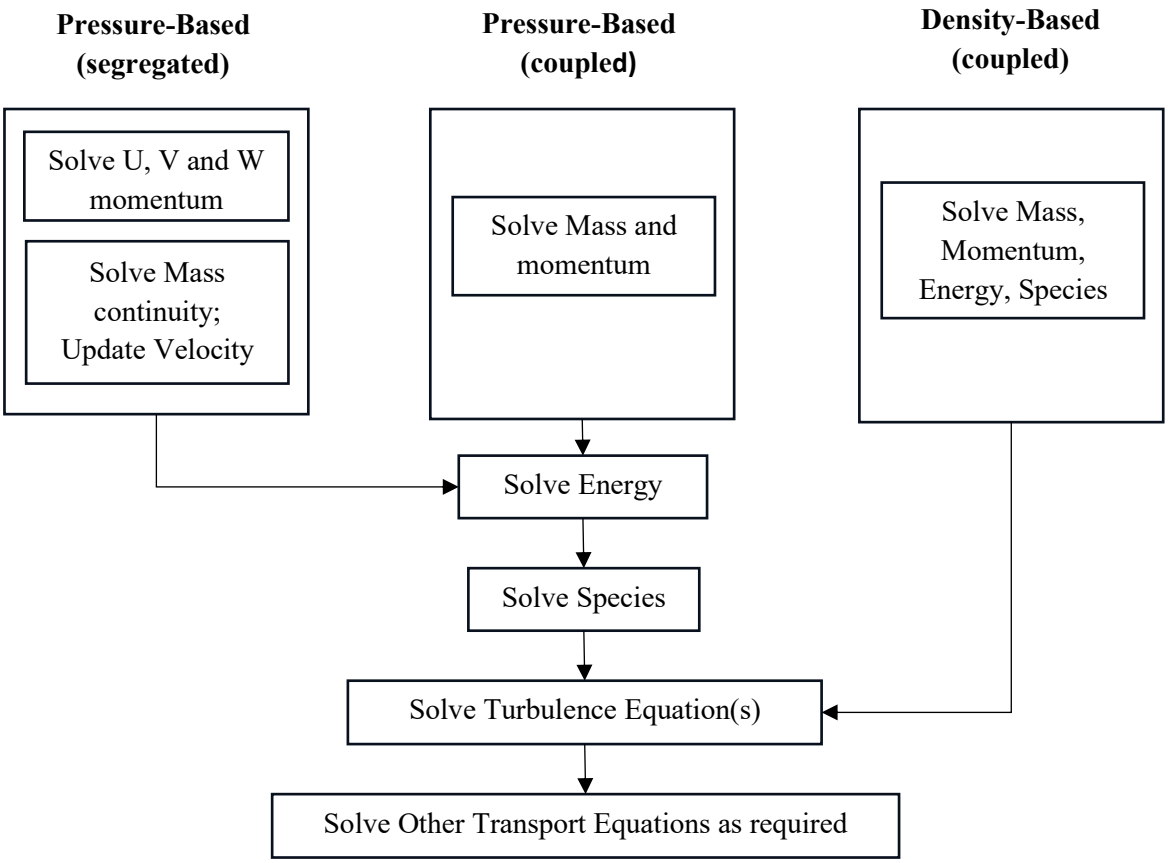

Figure III. 6: Different kinds of solver in FLUENT [33].

In our case, the Pressure Based solver is chosen and the sketch down shows the basic workflow for a simulation using ANSYS-Fluent software, The pressure-velocity coupling is employed in order to solve the SIMPLE algorithm.

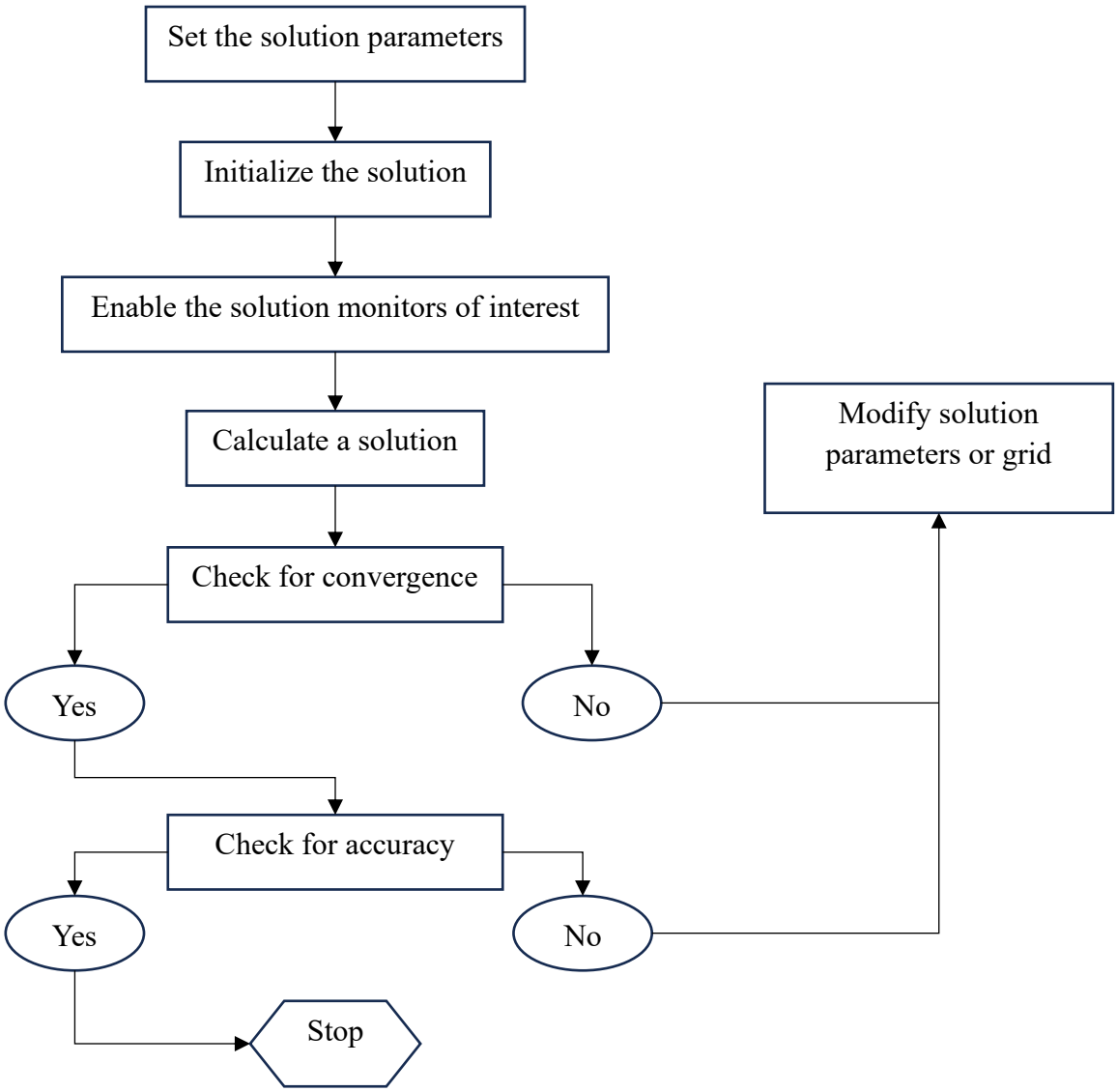

Figure III. 7: Resolution algorithm.

III.6 Conclusion:

This chapter provided an overview of principle of numerical computation. We then delved deeper into the finite volume method, the chosen method for this study. We explained its intricacies and the discretization schemes employed. Additionally, we introduced the ANSYS Fluent code as the tool for our numerical simulation.

In the next chapter and after choosing the mesh that will continue our study on it, we will present our numerical simulation results, their discussions and their validation.

Chapter IV
Results and Discussions

Introduction:

This chapter investigates the flow behavior of various fluids through an axisymmetric sudden expansion using numerical simulations using ANSYS-FLUENT. We explore the behavior of Newtonian fluids and non-Newtonian fluids, specifically viscoplastics modeled by the Bingham and Herschel-Bulkley models. The simulations encompass a range of Reynolds numbers Re ∈ [1, 200] and conducted with distinct power-law indices (n = 0.6, 0.8, 1 and 1.2).

The initial focus is on comparing the velocity fields of Newtonian and non-Newtonian fluids within the expansion. The results will be compared with those obtained by other researchers for the validation. We will then extend our study to analyze non-Newtonian fluids. Additionally, we will investigate velocity profiles at various positions within the flow, and examine vortex zones in each case by visualizing their contours. Finally, we will analyze head loss.

IV.1 Mesh studies:

in this work, we created 3 meshes and study each one this operation involves scrutinizing the mesh's impact on the outcome to ensure a closer result. the optimal mesh selection is paramount as it directly correlates with heightened accuracy, thereby increasing the reliability of the simulation outcomes.

The table IV.1 shows the mesh details for the three configurations:

MESH		**M-I**	**M-II**	**M-III**
STATISTICS	Nodes	23297	90113	621249
	Elements	21760	87040	205504

Table IV.1: The statistics of the three meshes.

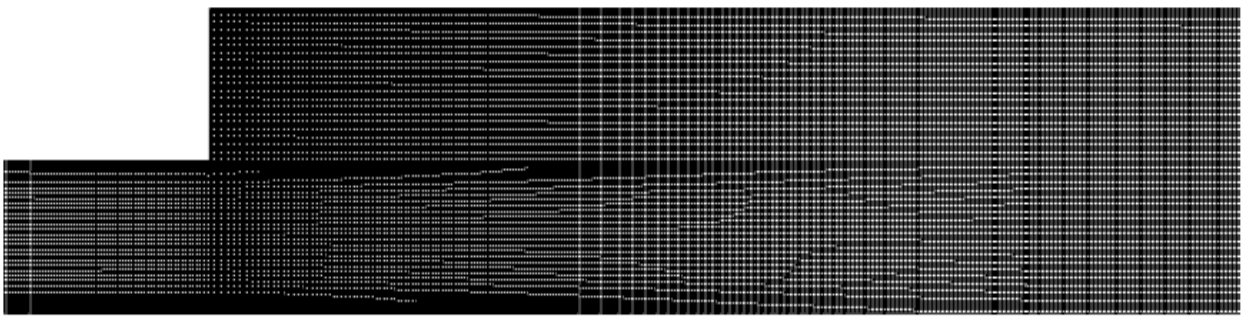

Figure IV.1: The mesh III as an example.

IV.2 Validation:

The validation of the numerical results of this work obtained by the ANSYS fluent software and illustrated by Figures IV.1, IV.2 and IV.3, first the mesh sensitivity tests were done with different cell numbers to see the evolution of the recirculation length L_v downstream of the pipe for a Newtonian fluid as a function of Reynolds number ($0 \leq Re \leq 200$).

Figure IV.1 illustrates the variation in recirculation length L_v as a function of the Reynolds number of the three meshes compared to the study by Evan Mitsoulis [11]. For $Re \leq 50$ there is no significant change so there is a good agreement for the three meshes. For $Re \geq 50$ there is a slight difference between the three configurations, especially for M-I.

The M-I and M-II meshes show relatively incompatible results since Re=50 and Re=100. The M-III mesh shows excellent agreement with Evan Mitsoulis's results [11] that it is very close.

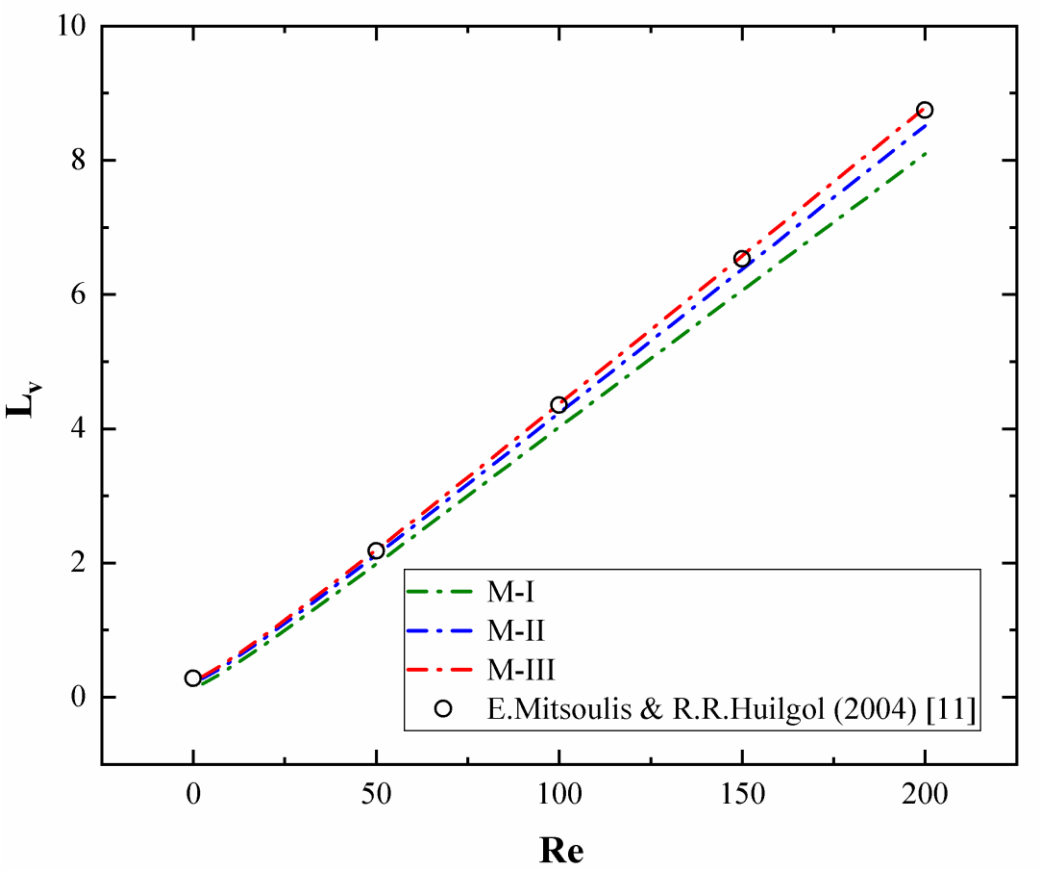

Figure IV. 2 : Variation of the vortex length as a function of Reynolds number.

Overall, the M-III mesh is a good match for Newtonian flow.

Figure IV.2.a and Figure IV.2.b compare our research results on the variation of vortex length L_v as a function of the Bingham number [0,2] for a specific Reynolds number (Re) of 50 with those of K. Hammad [12] according to Bingham and Herschel-Bulkley model with n=1 and n=1.2. Although the two curves show the same variation, there is however a slight difference for the value of the recirculation length. Indeed, our results show that the values are slightly lower than those of [12]. This difference is attributed to the choice of the position of the inlet section difference in the inlet section, it is at x=-25 for the present study and x=0 for that of [12].

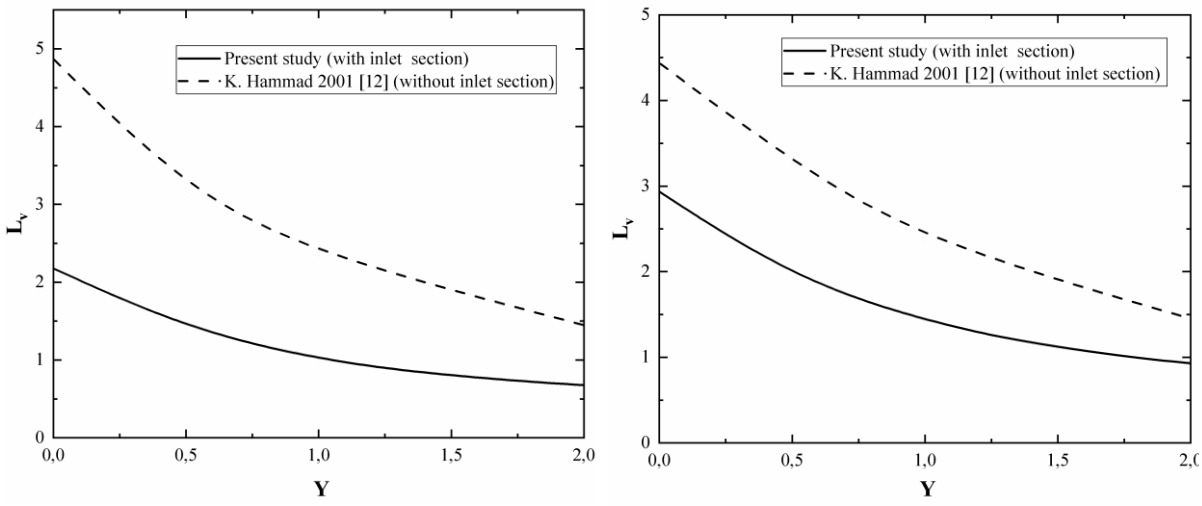

a) **b)**

Figure IV.3: Comparison of vortex length as a function of Yield number at Reynolds 50

a) n=1; b) n=1.2

Figure IV.3.a shows how the length of the recirculation zone, L_v, varies with fluctuations in the Yield number, Y, for a viscoplastic fluid for different values of the Reynolds number. Figure IV.3.b shows the variation of the ψ* intensity of the vortex in the recirculation zone as a function of the Bingham number for different values of the Reynolds number. there is a very good agreement between the numerical results of this study and those of Evan Mitsoulis [11].

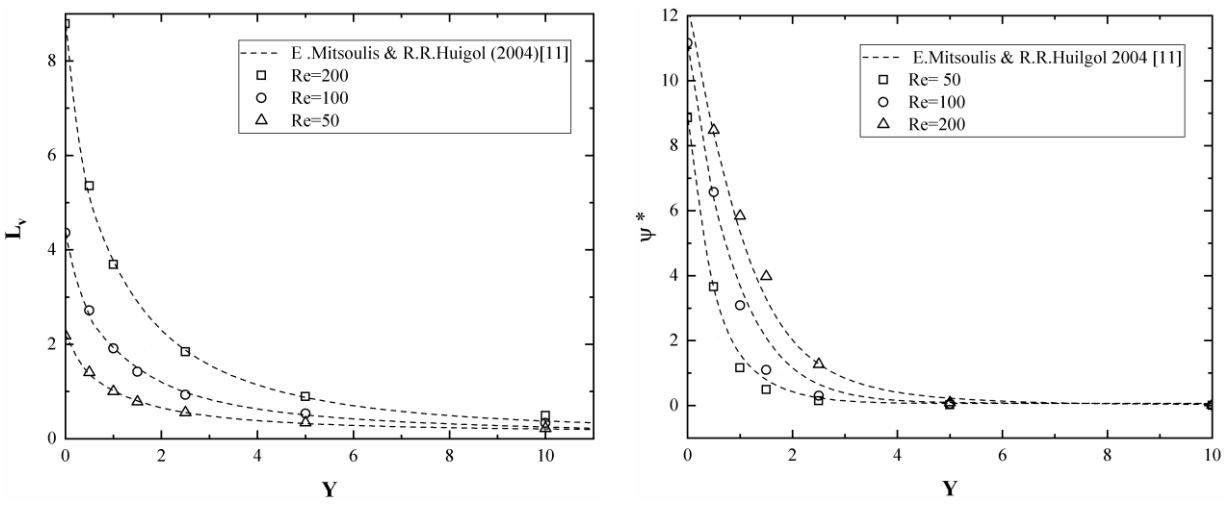

a) **b)**

Figure IV.4: Variation of length and intensity of the vortex as a function of Yield number.

IV.3 Upstream fully developed profiles:

Figure IV.4 shows the fully developed velocity profiles at the exit of the pipe for different yield numbers and power low index, for $Y = 0$ and $n = 1$. we see clearly the Newtonian behavior in pipe flow where the value of $u / U_i = 2$, it is noteworthy that the velocity profile for n=1 perfectly coincides with that of a Newtonian fluid in laminar flow according to the following equation:

$$\frac{u(r)}{U_{max}} = 1 - \frac{r^2}{R^2} \qquad \text{(IV.1)}$$

Which has parabolic profile. As n decreases, the velocity profile flattens near the axis of symmetry.

In return, as clearly seen the presence of a plug region around the centerline; the radial extent of this plug region increases with an increase in yield number and a decrease in power-law index outside the plug-flow region the velocity decreases rapidly to zero [12]. The velocity gradient close to the wall is greater for smaller power-law exponents and higher yield numbers as clearly demonstrated.

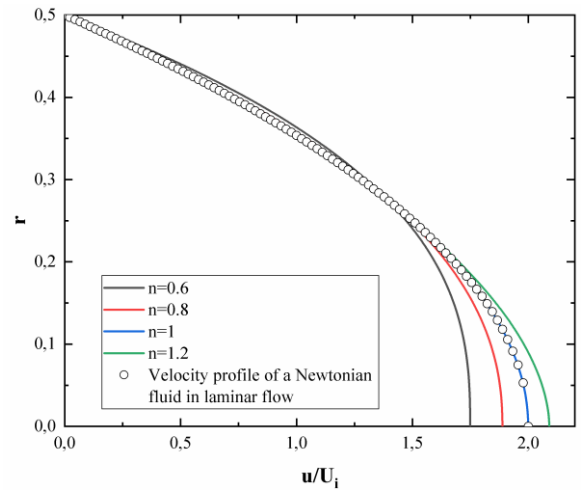
r
u/U_i
n=0.6
n=0.8
n=1
n=1.2
Velocity profile of a Newtonian fluid in laminar flow

a)

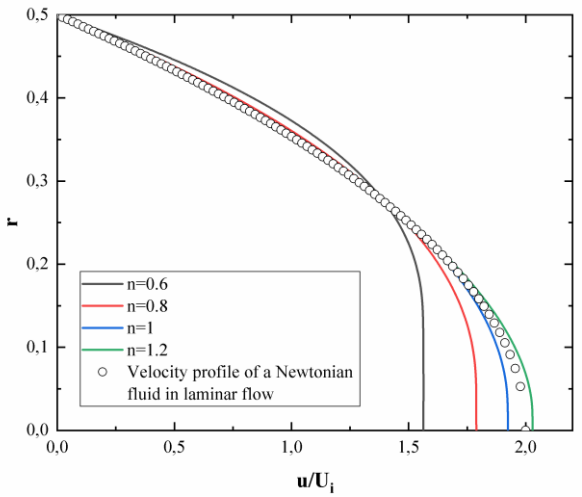
r
u/U_i
n=0.6
n=0.8
n=1
n=1.2
Velocity profile of a Newtonian fluid in laminar flow

b)

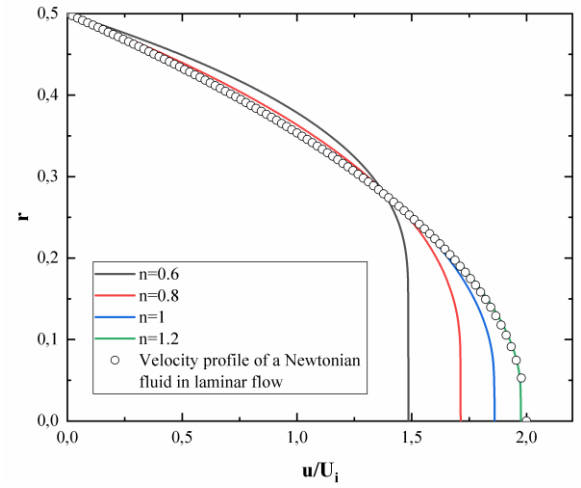
r
u/U_i
n=0.6
n=0.8
n=1
n=1.2
Velocity profile of a Newtonian fluid in laminar flow

c)

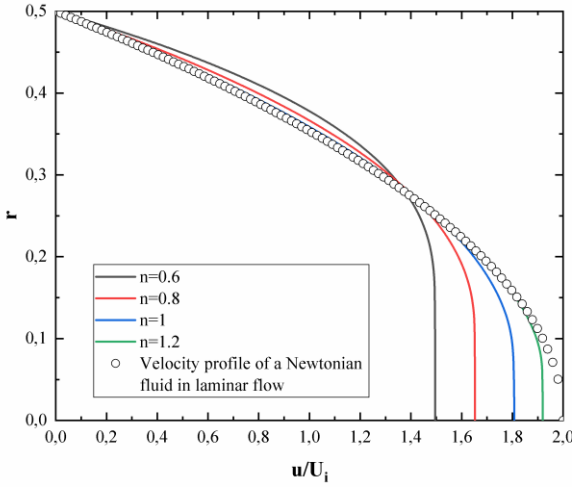
r
u/U_i
n=0.6
n=0.8
n=1
n=1.2
Velocity profile of a Newtonian fluid in laminar flow

d)

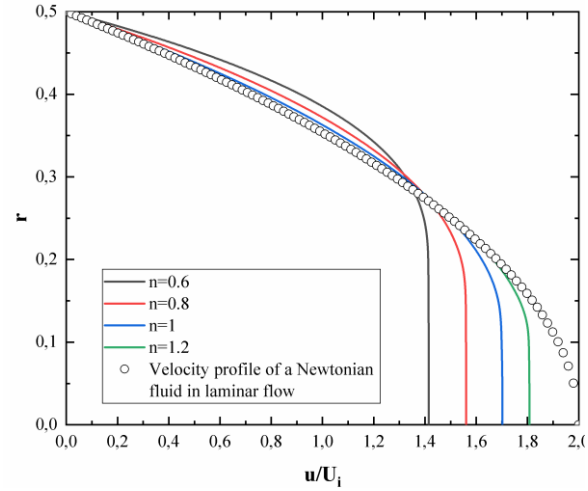
r
u/U_i
n=0.6
n=0.8
n=1
n=1.2
Velocity profile of a Newtonian fluid in laminar flow

e)

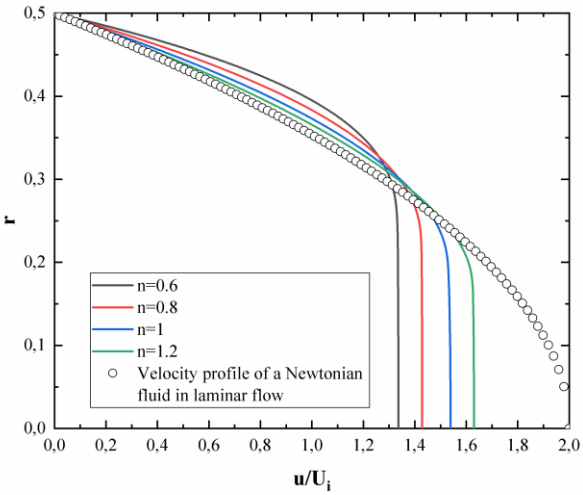
r
u/U_i
n=0.6
n=0.8
n=1
n=1.2
Velocity profile of a Newtonian fluid in laminar flow

f)

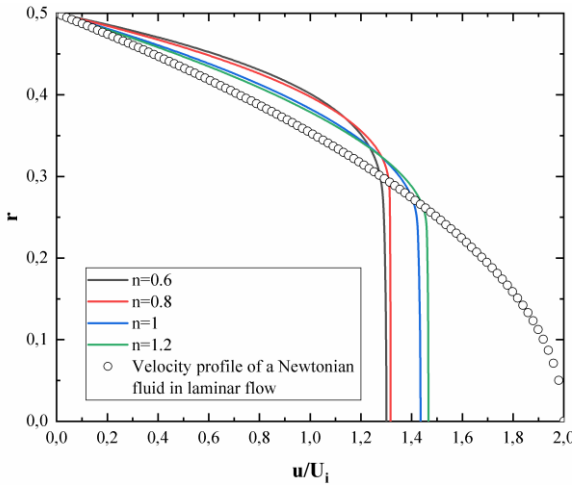

g)

Figure IV.5: Fully developed velocity profiles for different of Yield number.

a) Y=0; b) Y=0.5; c) Y=1; d) Y=1.5; e) Y=2.5; f) Y=5; g) Y=10

IV.4 Downstream fully developed profiles:

➢ Variation of Reynolds number:

As illustrated in Figure IV-5 the developing profiles of the streamwise velocity downstream of the expansion for two pairs of Reynolds, for different positions x of the axis of symmetry of the singularity X. We note that increasing the Reynolds number leads to a decrease in velocity and the appearance of a plug flow, which is greater in the case of Re=200. A comparison of the two graphs shows that the vortex zone depends on the Reynolds number, with the recirculation zone increasing as the Reynolds number increases.

The zoomed-in part of the velocity profiles shows that the velocity becomes negative, indicating a flow reversal. This flow reversal persists as the Reynolds number increases. Further downstream, the negative velocity region shrinks and the flow reattaches, becoming entirely forward with positive velocity. In certain position, we can observe a state of complete motionlessness. These areas correspond to the presence of solid zones within the vortex (Figure IV.11).

Eventually, the flow fully develops again, displaying a central plug flow region and a shear flow region [13].

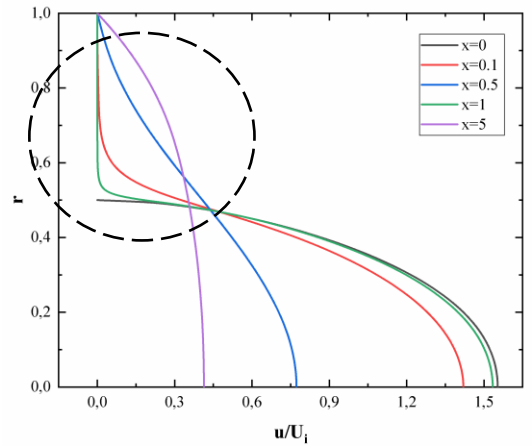

a) Re=1

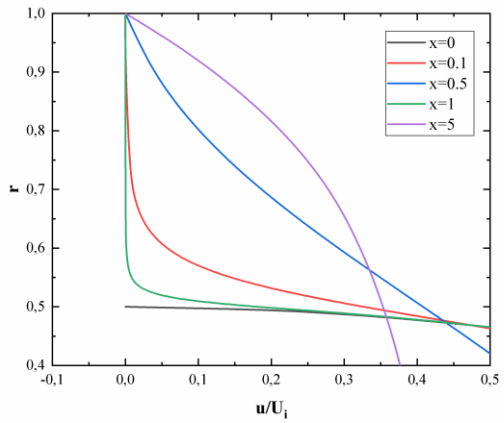

zoomed-in part of Re=1

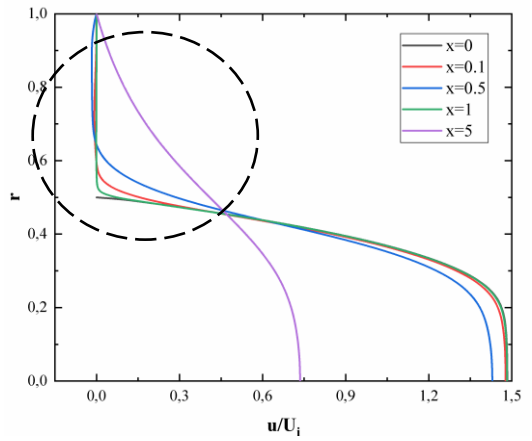

b) Re=200

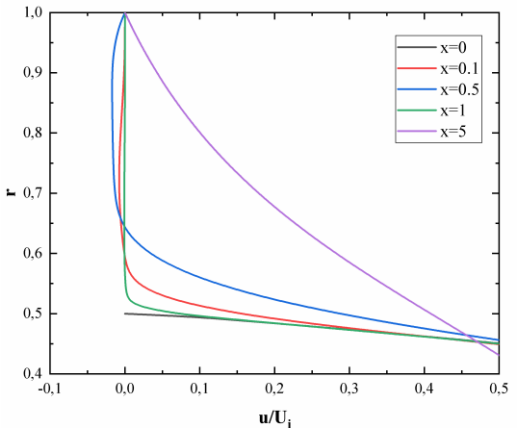

zoomed-in part of Re=200

Figure IV. 6: Investigation of velocity profiles versus radial position downstream of an expansion at Re=1, Re=200, Y=0,5 and n=0,6

- **Variation of Yield number:**

As a function of Yield number Y, Figure IV.6 depicts the variation of the velocity profile. It can be seen that these profiles have the same appearance except for the case of a Newtonian fluid, where these profiles are parabolic. For n=1,2, the profiles also have the same shape and show a flattening at the center of the pipe, this plug region increases when the Yield number Y increases. The change in flow direction (negative velocity) is only obtained in the case of Newtonian fluid (Figure IV.11).

Another noteworthy point from the figure is that as the Yield number Y increases, the speed of the flattening decreases.

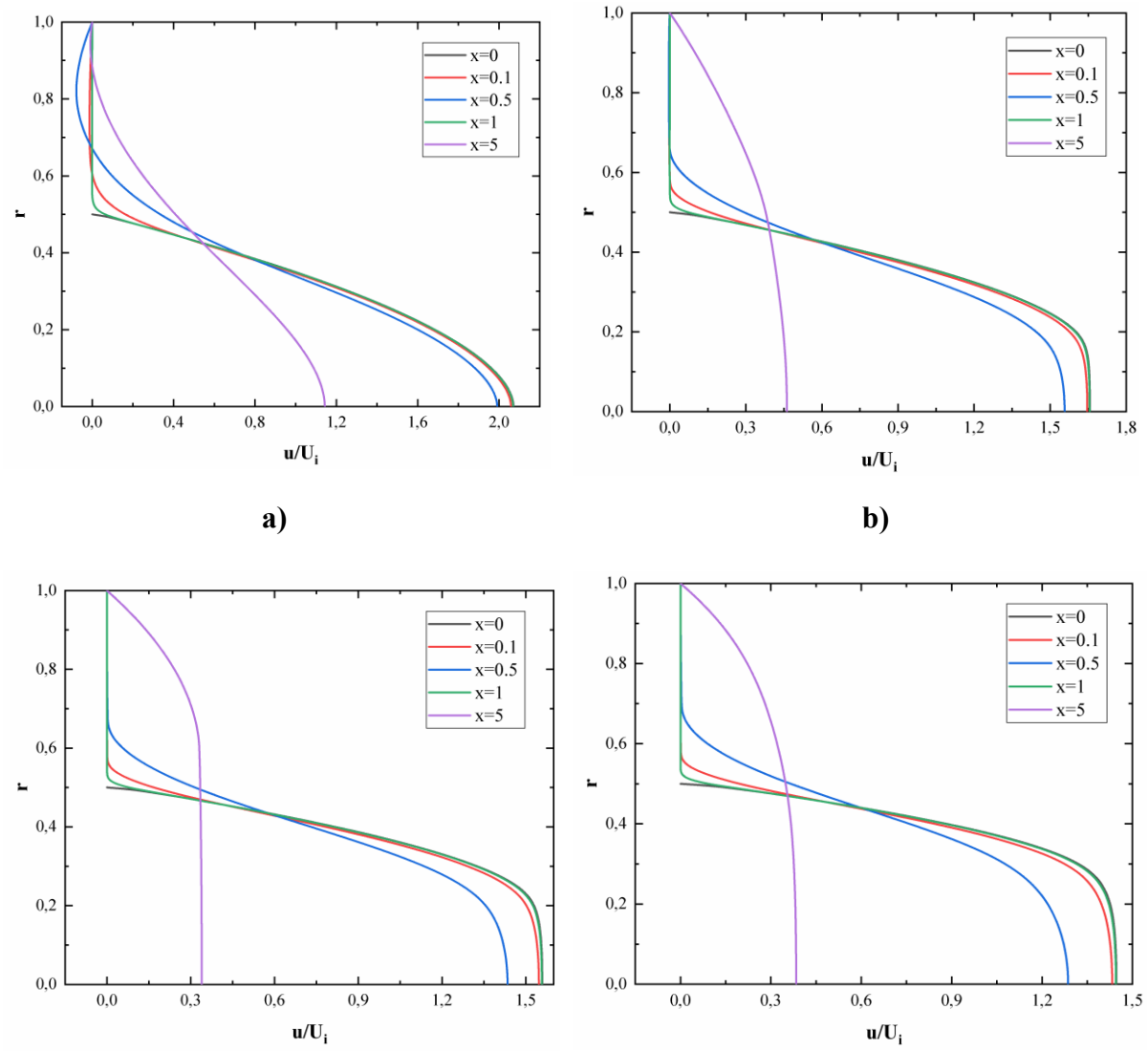

Figure IV.7: Investigation of velocity profiles versus radial position downstream of an expansion at Re=100, n=1,2. **a) Y=0; b) Y=2.5; c) Y=5; d) Y=10**

➢ Variation of power-low index:

As depicted in Figure IV-7, the dimensional velocity profile varies as a function of radius. Interestingly, with increasing values of the power-law index n, the velocity profiles become closer together, almost superimposing each other for n=1.2 for all positions. As the power-law index n increases, the velocity increases. This is due to the structure becoming more fluid, also we can see in (Figure IV.12)

These results remain valid for the different values of Reynolds number Re used in this numerical study.

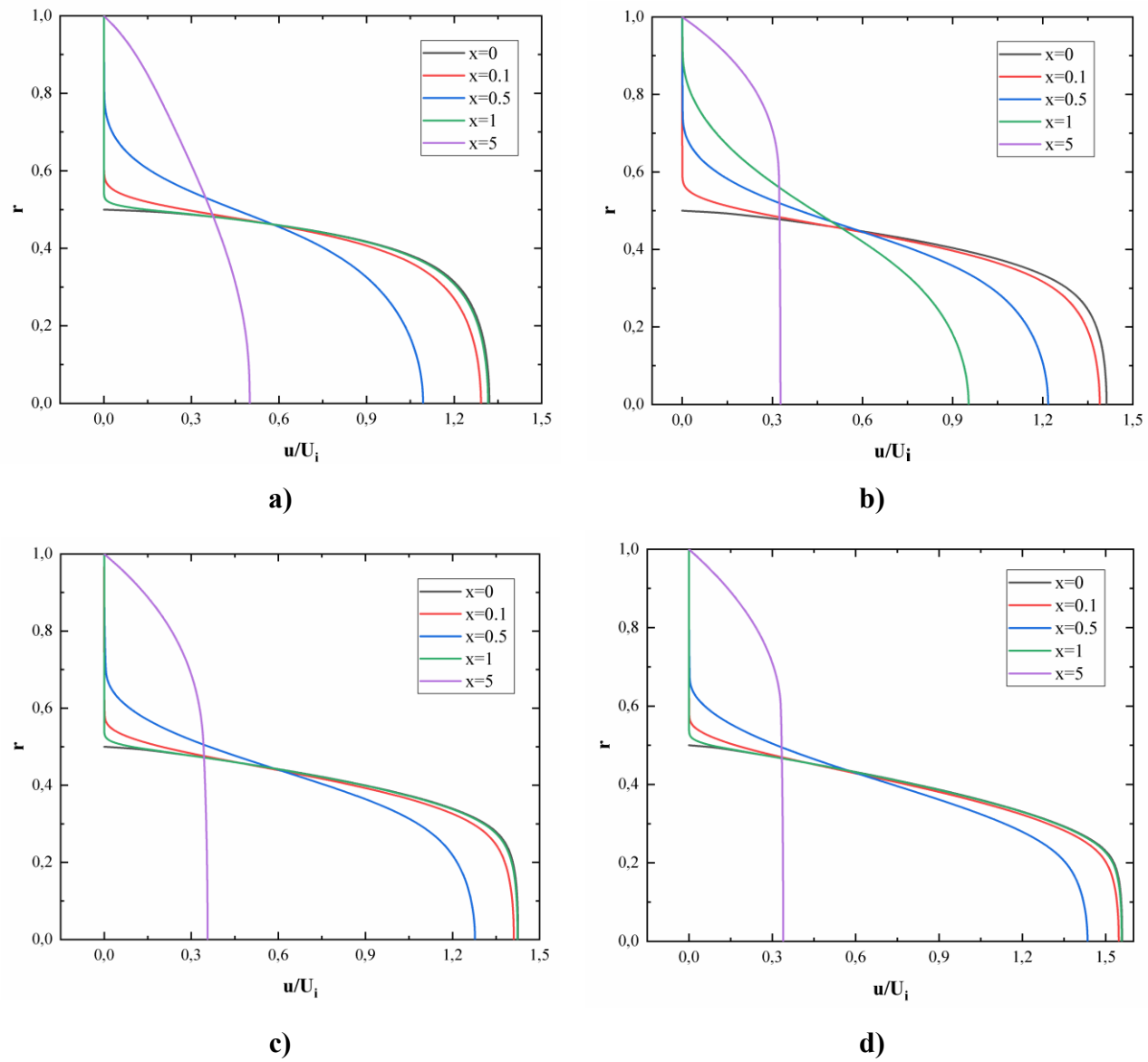

Figure IV.8: Investigation of Velocity Profiles versus Radial Position Downstream of an expansion at Re=100, Y=5. **a) n=0.6; b) n=0.8; c) n=1; d) n=1.2**

IV.5 Study of the vortex zone:

As can be seen in figures IV.8 (a, b, c, and d) the variation in the length L_v of the vortex as a function of the Yield number Y, for different values of the Reynolds number Re for a flow of viscoplastic fluid in a channel.

Notice that the length of the vortex decreases as the number of Yield Y increases. Similarly, this decrease in the length of the vortex is observed when the Reynolds number decreases. We also notice that the length of the vortex remains almost constant for Re = 1.

The length of the vortex also depends on the power-law index n, as it increases as the flow index increases, these results is similar to E. Mitsoulis's study[11].

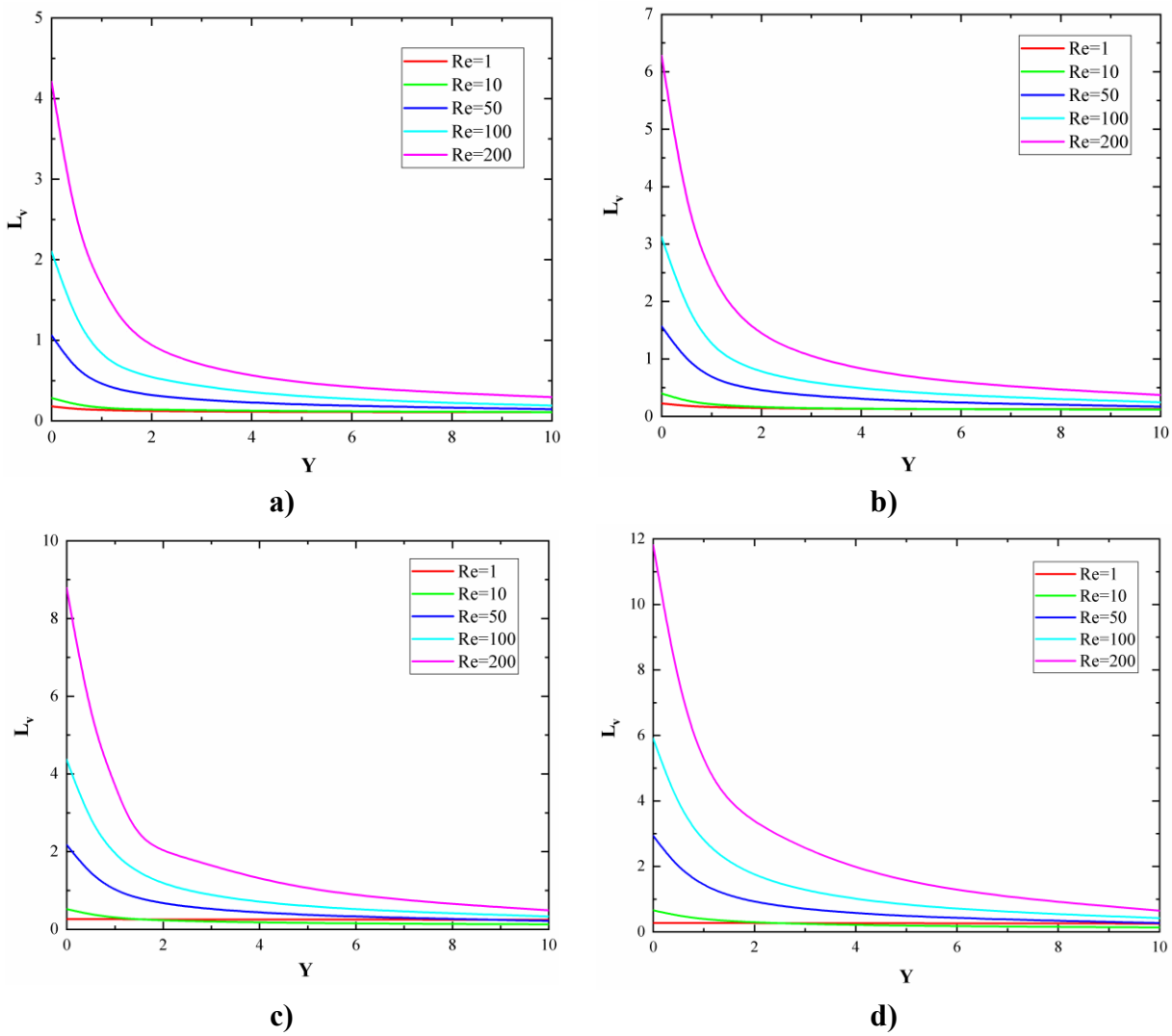

Figure IV.9: Evolution of the length of the vortex zone as a function of the Yield number and for different Reynolds numbers. **a) n=0.6; b) n=0.8; c) n=1; d) n=1.2**

Figures IV.9 (a, b, c, and d) show the variation in the intensity of the vortex area ψ* as a function of the Yield number Y, for different values of the Reynolds number Re for a flow of viscoplastic fluid in a channel.

Is noticeable that the intensity of the vortex zone ψ* drops rapidly and exponentially as Yield number Y increases [11]. Similarly, this decrease in the intensity of the vortex zone ψ* is observed when the Reynolds number decreases. It is also noticeable that the intensity of the vortex zone ψ* remains almost constant for Re = 1.

The intensity of the vortex zone ψ* also depends on the power-law index n, as it increases as the flow index increases [11].

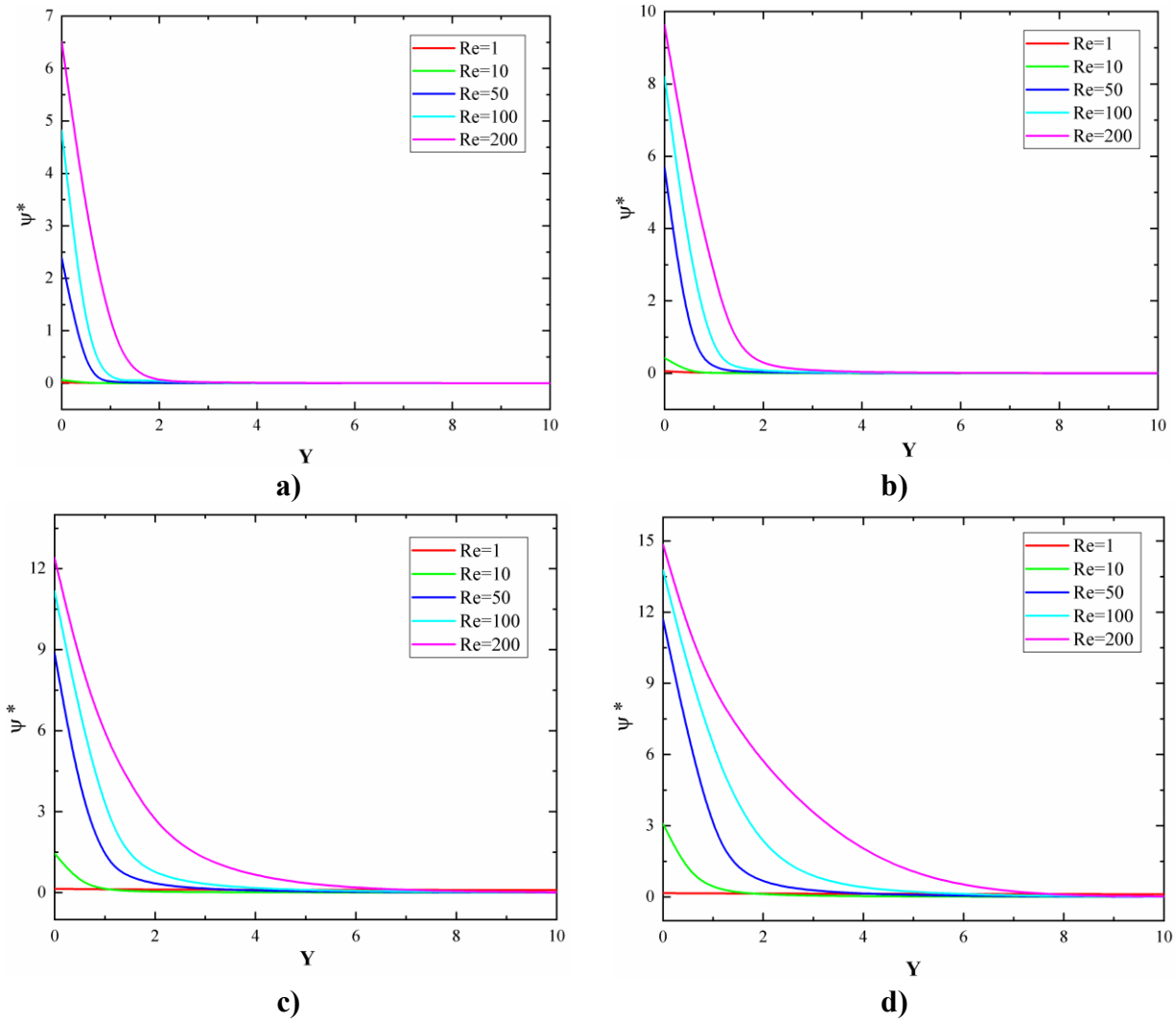

Figure IV.10: Evolution of the intensity of the vortex zone as a function of the Yield number for different Reynolds numbers. **a) n=0.6; b) n=0.8; c) n=1; d) n=1.2**

As shown in Figure IV.10 the variation of vortex length L_v as a function of the power-law index n. It can be observed that the length of the vortex L_v increases with increasing of the power-law index n and decreases with decreasing of Yield number Y. For the cases of Y=5 and Y=10, the minimum vortex length L_v remains constant, which can be attributed to the plug flow behavior.

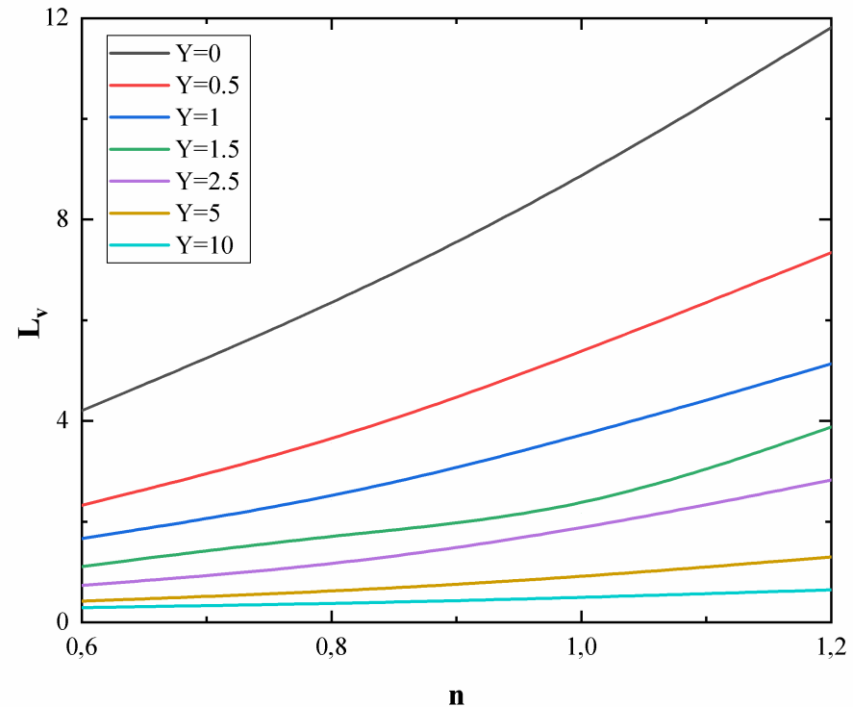

Figure IV.11: Evolution of the vortex zone length as a function of index for varying yield numbers Re=200.

IV.6 Contours:

➢ Variation of Yield number:

Figure IV.11 shows the contours, yielded and unyielded regions with stream functions of n=0,8; Re=100 and different Yield number.

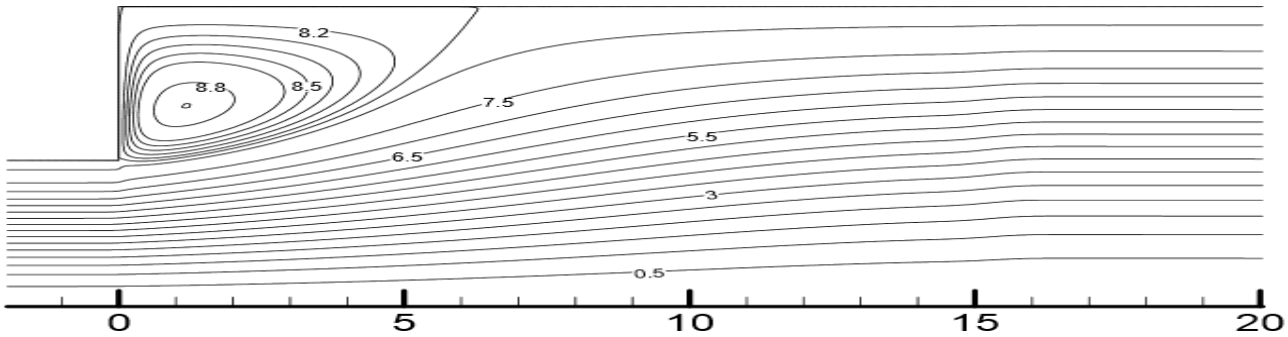

a) Y=0

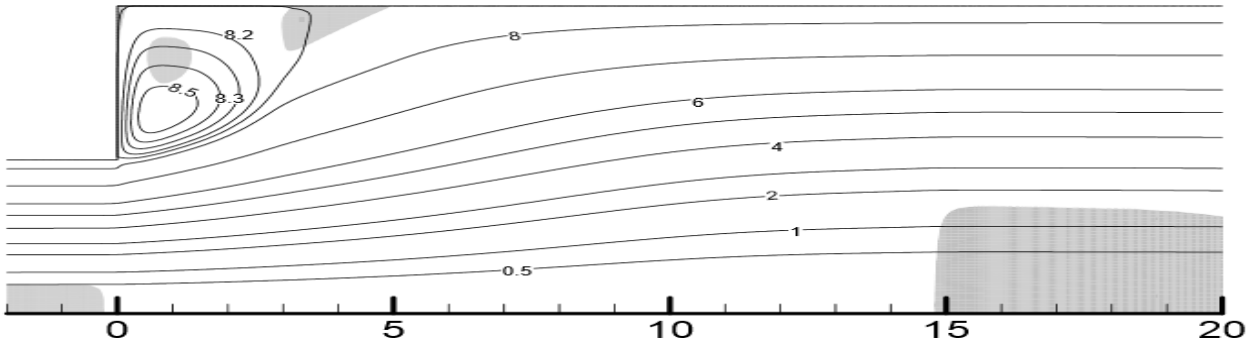

b) Y=0.5

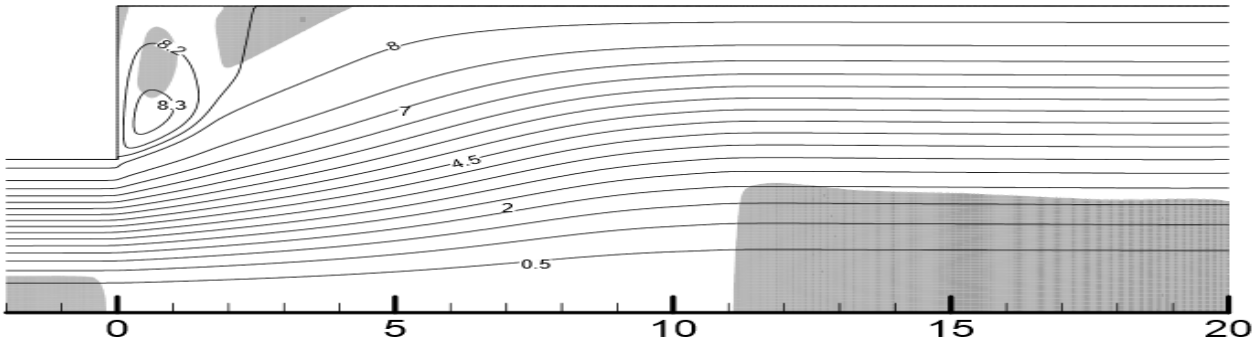

c) Y=1

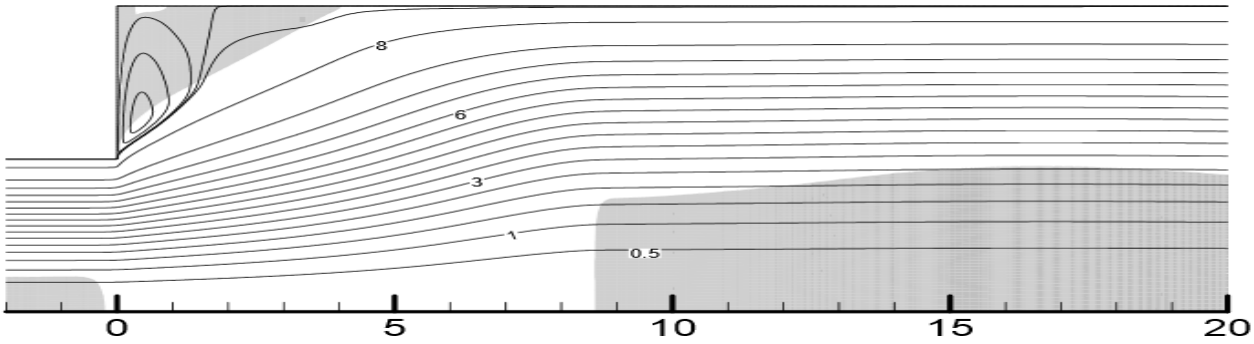

d) Y=1.5

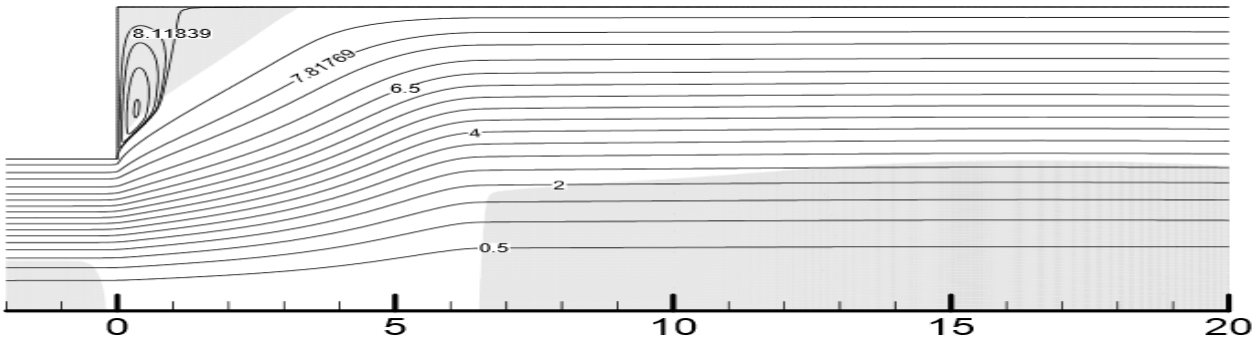

e) Y=2.5

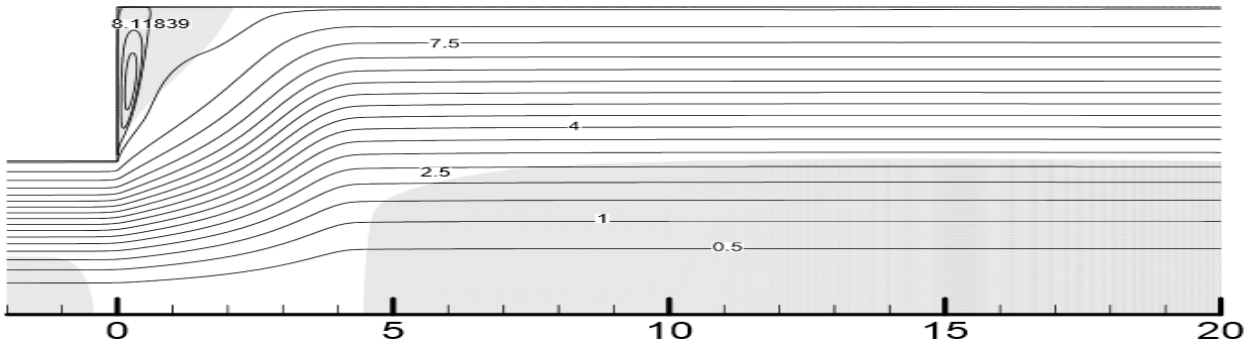

f) Y=5

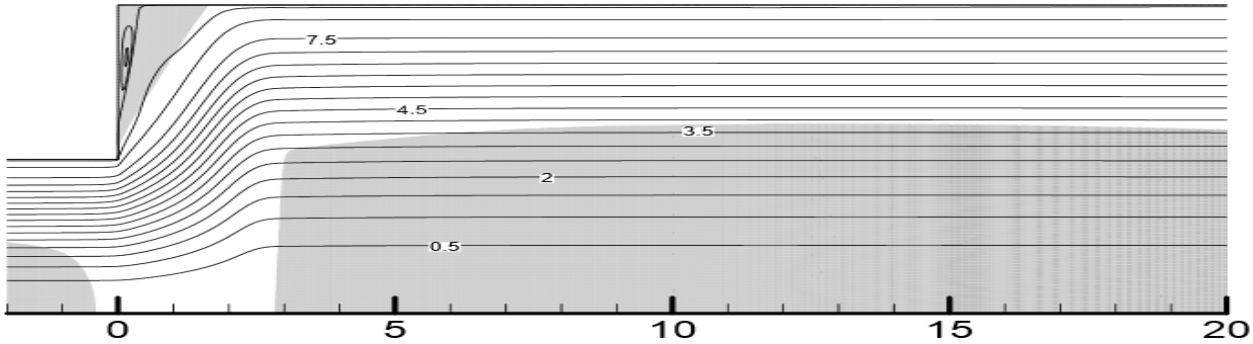

g) Y=10

Figure IV.12: Yielded and unyielded regions with stream functions of n=0,8; Re=100 and different Yield number.

- **Variation of power-low index:**

Figure IV.12 shows the contours, yielded and unyielded regions with stream functions of Y=2,5; Re=100 and different Power low index.

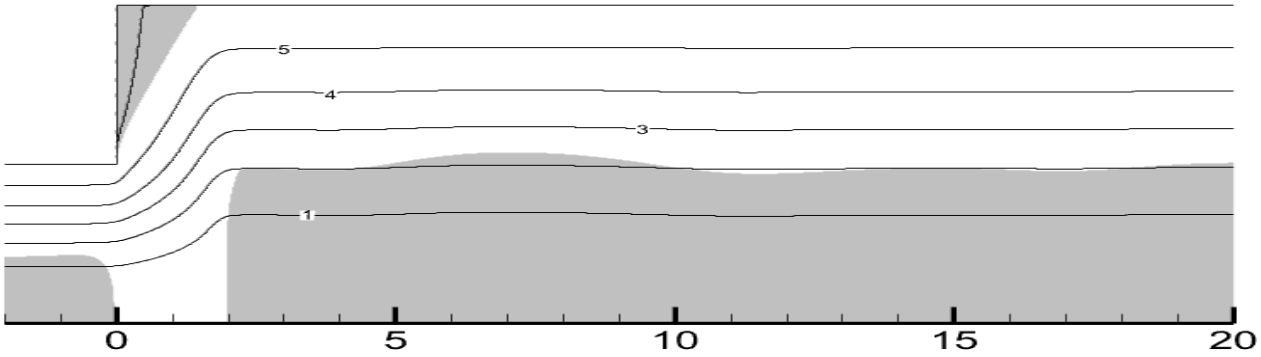

a) n=0,6

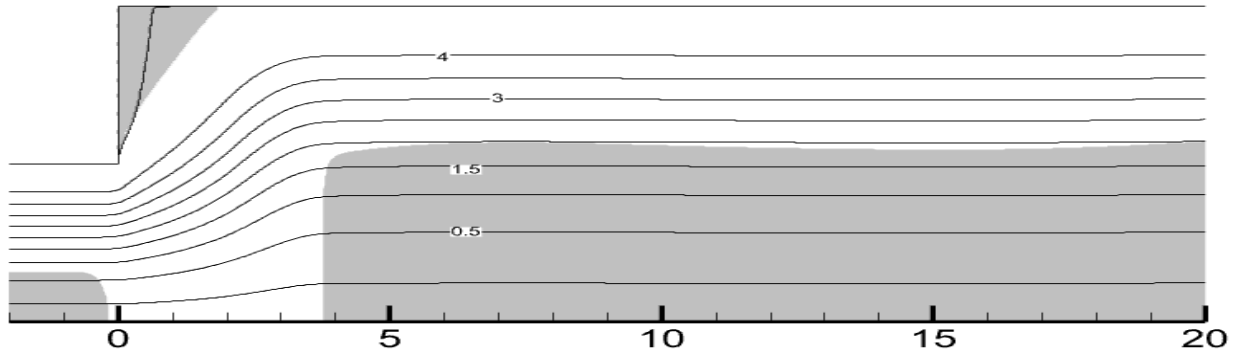

b) n=0,8

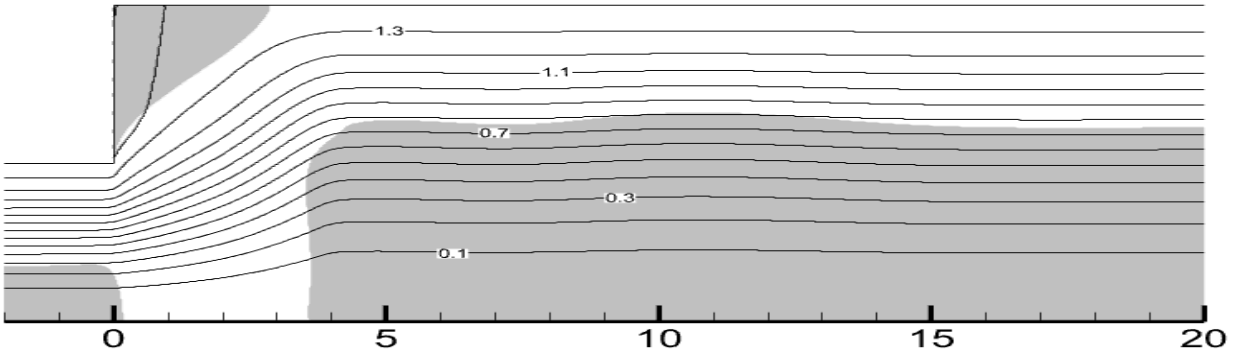

c) n=1

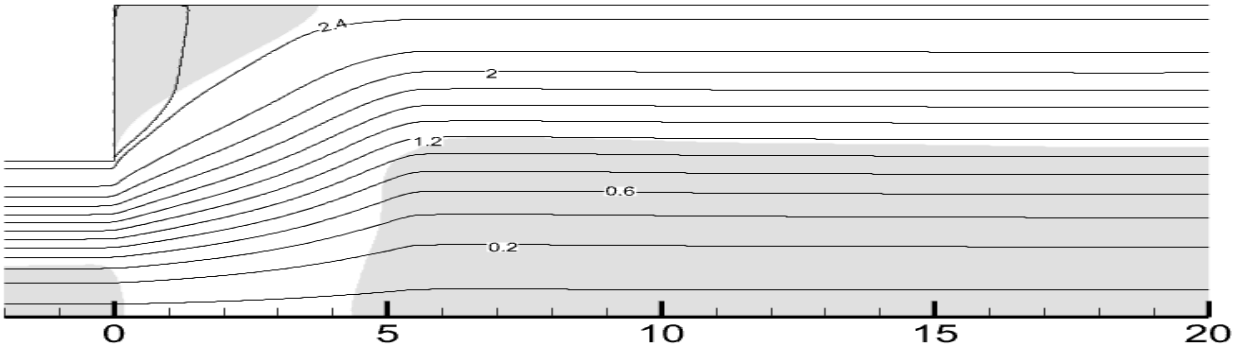

e) n=1,2

Figure IV.13: Yielded and unyielded regions with stream functions of Y=2,5; Re=100 and different Power low index.

IV.7 Flow Development along the pipe:

As depicted in Figure IV.13, the dimensionless velocity profile varies along the axis of symmetry x. Upstream of the expansion x<0, the velocity reaches a constant maximum value. However, between x = 0 and x ≈ 5, a rapid decrease in velocity is observed due to recirculation. flow development is complete by around x<5, whereas for a Newtonian fluid, it takes about x>5 [13]. the velocity remains constant throughout the pipe. Notably, the magnitude of this

velocity decrease depends on the Yield number Y. Lower Yield Numbers Y exhibit a less pronounced decrease in velocity compared to higher values.

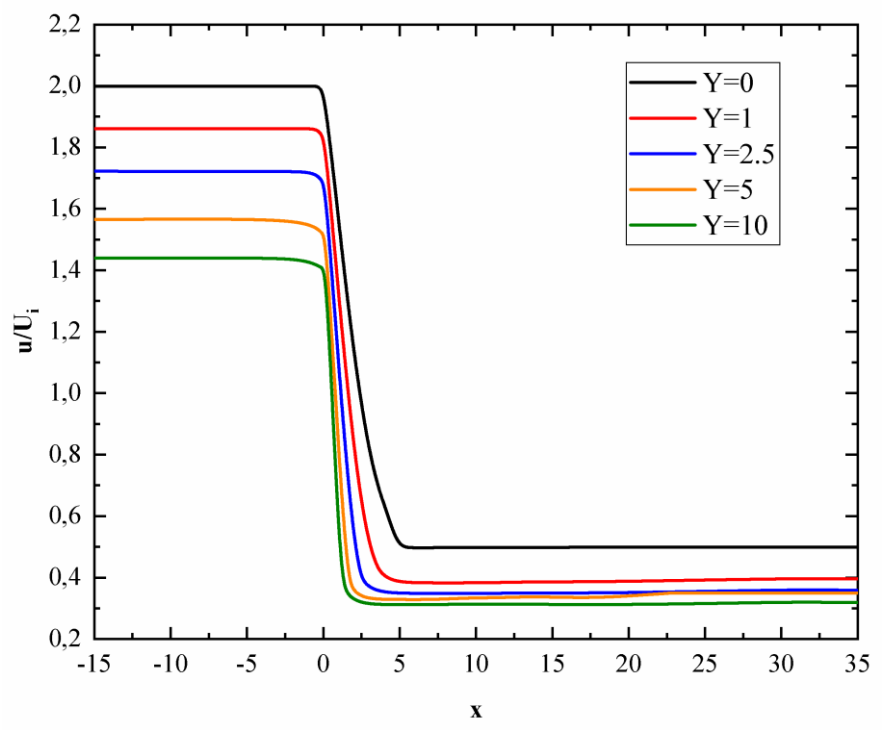

Figure IV.14: Variation of the velocity along the centerline of an expansion for different Yield numbers.

IV.8 Evaluation of pressure-loss:

Figure IV.14 illustrates how pressure changes along the centerline of the pipe, represented by the x-axis. Before the expansion $x \leq 0$, the pressure increases steadily. As the fluid flows past the point of expansion $x \geq 0$, the pressure initially shows a small increase. This is followed by a steady decrease in pressure as the fluid encounters the wider section. Further downstream (beyond the expansion), the pressure eventually returns to a constant value again [22].

The figure also reveals another interesting observation. The size of the recirculation zone, a pocket of slow-moving fluid, is influenced by the index n, which relates to the flow behavior of the fluid. We observed that this zone gets larger with fluids that have a different power-law index n compared to standard fluids.

This suggests the presence of an additional pressure loss within the recirculation zone, known as "irreversible pressure loss" found by Oliveira [23]

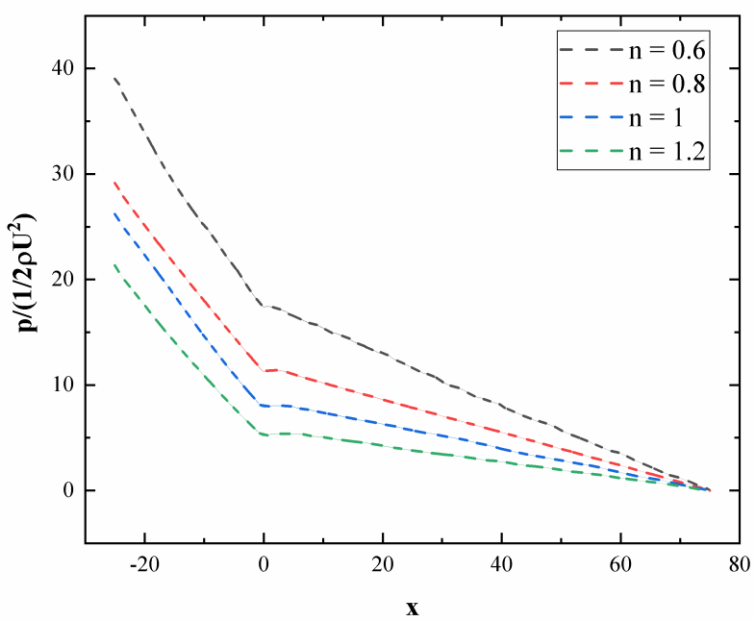

Figure IV.15: Normalized pressure variation along the centerline of the pipe for different power-law index.

As for the Figure 14 that shows the variation of the pressure coefficient as a function of the position x on the axis of symmetry, with the Yield number Y increases. the head loss increases. This results also shows in Oliveira's article [23].

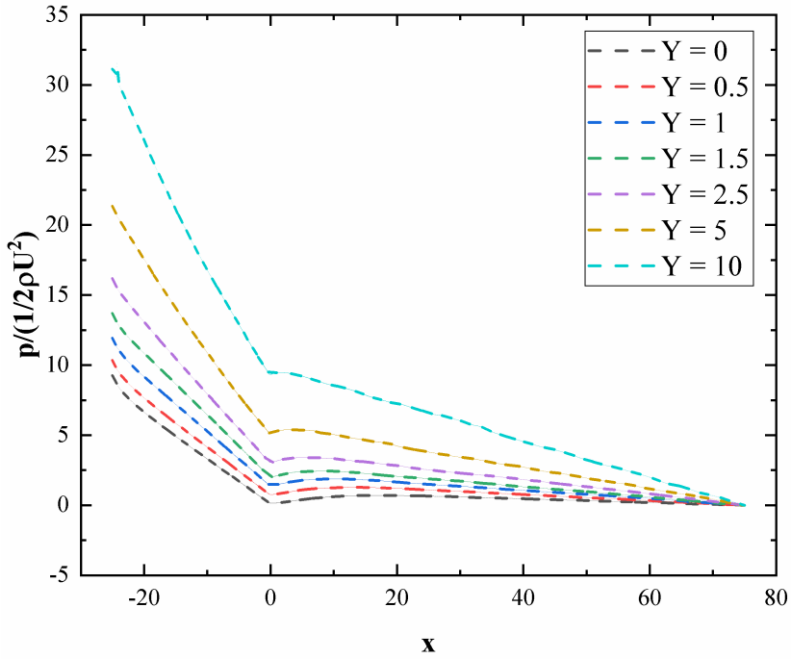

Figure IV.16: Normalized pressure variation along the centerline of the pipe for different Yield number.

IV.8 Conclusion:

Our initial comparisons of the velocity fields of Newtonian and non-Newtonian fluids within the expansion have been validated against previous research findings, ensuring the reliability of our simulations. Extending our study to non-Newtonian fluids, we have meticulously analyzed the velocity profiles at various positions within the flow and examined the vortex zones by visualizing their contours. This has provided a deeper understanding of the complex flow dynamics in sudden expansions.

Furthermore, our analysis of head loss has highlighted the differences in energy dissipation between Newtonian and non-Newtonian fluids, offering valuable insights for practical applications. Overall, this chapter's findings contribute significantly to the existing knowledge of fluid flow through expansions, advancing the capabilities of numerical simulations in fluid dynamics.

General Conclusion

In this thesis, we conducted a numerical investigation of viscoplastic fluid flow through a sudden expansion using a numerical simulation. This study allowed us to enhance our understanding of viscoplastic fluid flows and examine the behavior of these fluids in a singular geometry.

The study was carried out for intermediate Reynolds and yield numbers, with a particular focus on geometric conditions. The numerical simulation was performed using the ANSYS Fluent code and employing the finite volume method.

Initially, we numerically investigated the flow of Newtonian and viscoplastic fluids through a sudden expansion. The influence of meshing on the results was also examined.

The findings of this study are consistent with those of other numerical and experimental studies on viscoplastic flow through simple geometries. Excellent agreement was observed. Our results can be utilized to improve the design of reactors and other industrial equipment where viscoplastic flows are prevalent.

The effect of Reynolds number on recirculation zones was investigated and confirmed for both Newtonian and viscoplastic fluid flows. For yield number, the findings of this study demonstrate an opposing effect to that of Reynolds number on recirculation zones, flow redevelopment downstream of the step, and the emergence of solid zones in the flow. These zones were also affected by Reynolds number and power low indices.

These findings were used to develop numerical correlations based on rheological and geometrical parameters for predicting the length and intensity of the recirculation zone. The pressure drop across the expansion was also investigated.

References

References

[1] B. R. Munson, A. P. Rothmayer, et T. H. Okiishi, *Fundamentals of Fluid Mechanics, 7th Edition*. Wiley, 2012.

[2] K. R. Symon, *Mechanics*. Reading, Mass. : Addison-Wesley Pub. Co., 1971.

[3] « Bingham yield stress and Bingham plastic viscosity of homogeneous Non-Newtonian slurries | Semantic Scholar ».

[4] T. Ghosh, D. Prasad, N. Dutt, et K. Y. Rani, *Viscosity of Liquids: Theory, Estimation, Experiment, and Data*. 2007. doi: 10.1007/978-1-4020-5482-2.

[5] B. Guo, X. Liu, et X. Tan, *Petroleum Production Engineering*. Elsevier Science, 2017.

[6] A. B. Metzner et J. C. Reed, « Flow of non-newtonian fluids—correlation of the laminar, transition, and turbulent-flow regions », *AIChE Journal*, vol. 1, nº 4, p. 434-440, déc. 1955, doi: 10.1002/aic.690010409.

[7] R. P. Chhabra et J. F. Richardson, « Chapter 1 - Non-Newtonian fluid behaviour », in *Non-Newtonian Flow in the Process Industries*, R. P. Chhabra et J. F. Richardson, Éd., Oxford: Butterworth-Heinemann, 1999, p. 1-36. doi: 10.1016/B978-075063770-1/50002-6.

[8] C. Rigal, « Comportement de fluides complexes sous écoulement : approche expérimentale par résonance magnétique nucléaire et techniques optiques et simulations numériques », phdthesis, Université de Lorraine, 2012.

[9] E. W. Merrill, A. M. Benis, E. R. Gilliland, T. K. Sherwood, et E. W. Salzman, « Pressure-flow relations of human blood in hollow fibers at low flow rates », *J Appl Physiol*, vol. 20, nº 5, p. 954-967, sept. 1965, doi: 10.1152/jappl.1965.20.5.954.

[10] H. A. Barnes, « Thixotropy—a review », *Journal of Non-Newtonian Fluid Mechanics*, vol. 70, nº 1, p. 1-33, mai 1997, doi: 10.1016/S0377-0257(97)00004-9.

[11] E. Mitsoulis et R. R. Huilgol, « Entry flows of Bingham plastics in expansions », *Journal of Non-Newtonian Fluid Mechanics*, vol. 122, nº 1, p. 45-54, sept. 2004, doi: 10.1016/j.jnnfm.2003.10.007.

[12] K. J. Hammad, G. C. Vradis, et M. V. O¨tu¨gen, « Laminar Flow of a Herschel-Bulkley Fluid Over an Axisymmetric Sudden Expansion », *Journal of Fluids Engineering*, vol. 123, nº 3, p. 588-594, mars 2001, doi: 10.1115/1.1378023.

[13] G. C. Vradis, M. V. Otugen, G. C. Vradis, et M. V. Otugen, « The axisymmetric sudden expansion flow of a non-Newtonian viscoplastic fluid », *Journal of Fluids Engineering*, vol. 119, nº 1, Art. nº 1, janv. 1997.

[14] K. J. Hammad, M. V. O¨tu¨gen, G. C. Vradis, et E. B. Arik, « Laminar Flow of a Nonlinear Viscoplastic Fluid Through an Axisymmetric Sudden Expansion », *Journal of Fluids Engineering*, vol. 121, nº 2, p. 488-495, juin 1999, doi: 10.1115/1.2822235.

[15] K. Hammad, « Suddenly expanding recirculating and non-recirculating viscoplastic non-newtonian flows », *Journal of Visualization*, janv. 2015.

[16] M. Bekhadra, « Numerical correlations for Herschel bulkley fluid flow through an axisymmetric sudden expansion », *CERN European Organization for Nuclear Research - Zenodo*, oct. 2022.

[17] E. Hegaj et E. Borzenko, « Numerical Simulation of the Steady-State Herschel-Bulkley Fluid Flow in a Channel with Sudden Expansion », *KEM*, vol. 743, p. 474-479, juill. 2017, doi: 10.4028/www.scientific.net/KEM.743.474.

[18] M. Bekhadra, S. Chemloul, M. Abdelhak, et S. Bekhadra, *Intéressantes simulations de l'écoulement d'un fluide à seuil dans un élargissement et analyse de la perte de charge*. 2022.

[19] M. Bekhadra, N.-E. Chemloul, A. Menouer, et K. Chaib, « Numerical Study of Laminar Bingham Fluid in Axisymmetric Sudden Expansion », *International Journal of Heat and Technology*, vol. 40, p. 45-52, févr. 2022, doi: 10.18280/ijht.400106.

[20] F. S. F. Zinani, « Galerkin least-squares solutions for purely viscous flows of shear-thinning fluids and regularized yield stress fluids », 2013.

[21] F. Machado, F. Zinani, et S. Frey, « Herschel-Bulkley Fluid Flows Through a Sudden Axisymmetric Expansion via Galerkin Least-Squares Methodology ».

[22] A. Menouer, N. Chemloul, K. Chaib, et K. Ahmed, « Steady Flow of Purely Viscous Shear-Thinning Fluids in a 1:3 Planar Gradual Expansion », *Journal of Applied Fluid Mechanics*, vol. 12, p. 789-801, mai 2019, doi: 10.29252/jafm.12.03.29245.

[23] P. J. Oliveira et F. T. Pinho, « Pressure drop coefficient of laminar Newtonian flow in axisymmetric sudden expansions », *International Journal of Heat and Fluid Flow*, vol. 18, n° 5, p. 518-529, oct. 1997, doi: 10.1016/S0142-727X(97)80010-0.

[24] F. Irgens, *Rheology and Non-Newtonian Fluids*. Springer Science & Business Media, 2013.

[25] Y. A. Cengel et J. M. Cimbala, *Mécanique des fluides*. De Boeck Superieur, 2017.

[26] *Lesson 6, part 5: pipe flow velocity profile for a Bingham fluid*, (17 juillet 2020).

[27] S. Bahi et C. Menni, « Simulation des pertes de charges dans les conduites de distribution de gaz naturel », Thesis, université de bouira, 2017.

[28] S. Nguyen, « Dynamique d'une interface en présence d'une singularité de contact solide/fluide. ».

[29] O. Kolditz, *Computational Methods in Environmental Fluid Mechanics*. Berlin, Heidelberg: Springer, 2002. doi: 10.1007/978-3-662-04761-3.

[30] R. Eymard, T. Gallouët, et R. Herbin, « Finite volume methods », vol. 7, p. 713-1018, 2000, doi: 10.1016/S1570-8659(00)07005-8.

[31] « Thèse BEKHADRA Mokhtar.pdf ». Consulté le: 5 mai 2024. [En ligne]. Disponible sur: http://dspace.univ-tiaret.dz/bitstream/123456789/14371/1/Th%C3%A8se%20%20BEKHADRA%20Mokhtar.pdf

[32] M. B. Naceur, « Etude numérique de l'écoulement d'un fluide viscoplastique à travers une singularité : élargissement brusque ».

[33] « Lecture_7_Fluent_Solver_Settings.pdf ». Consulté le: 21 mai 2024. [En ligne]. Disponible sur: https://www.drahmednagib.com/CAD_2018/Lecture_7_Fluent_Solver_Settings.pdf

Abstract

A numerical analysis was performed to examine the behavior of the laminar flow of a Newtonian and non-Newtonian fluid through a sudden axisymmetric expansion, by varying the flow parameters such as the Reynolds number and yield number. This study, conducted using the software ANSYS Fluent, investigated the influence of these parameters on the fluid flow structure. The numerical results revealed that the recirculation zones have a length and intensity proportional to the Reynolds number, while they are inversely proportional to the yield number. In addition, the local pressure loss coefficient increases for Newtonian fluid, an effect that is also manifested in the case of viscoplastic fluid. Models such as the Bingham and Herschel-Buckley models have been developed to predict the recirculation lengths and intensities as well as the local (or singular) pressure loss coefficient for both types of fluid.

Keywords: Viscoplastic fluid, Sudden expansion, Yield number, power-low index, Recirculation, vortex zones, Local pressure drop coefficient

Résumé

Une analyse numérique a été réalisée pour examiner le comportement de l'écoulement laminaire d'un fluide newtonien et non newtonien à travers une élargissement axisymétrique et brusque, en faisant varier les paramètres adimensionnels d'écoulement tels que le nombre de Reynolds et le nombre de Bingham et Herschel-Buckley model. Cette étude, réalisée à l'aide du logiciel c ANSYS Fluent, a étudié l'influence des paramètres adimensionnels sur la structure de l'écoulement des fluides. Les résultats numériques ont montré que les zones de recirculation ont une longueur et une intensité proportionnelles au nombre de Reynolds, alors qu'elles sont inversement proportionnelles au nombre de Bingham et Herschel-Buckley model. En outre, le coefficient de perte de pression locale augmente pour le fluide newtonien, un effet qui se manifeste également dans le cas du fluide viscoplastique. Des modèles comme Bingham et Herschel-Buckley ont été développés pour prédire les longueurs et l'intensité de recirculation ainsi que le coefficient de la perte de pression locale (ou singulière) pour les deux types de fluide.

Mots-clés : Fluide viscoplastique, élargissement brusque, nombre de Bingham et Herschel-Buckley model, indice d'écoulement, recirculation, vortex zones, Coefficient de perte de charge locale.

ملخص

تم إجراء تحليل عددي لفحص سلوك التدفق الصفحي لسائل نيوتوني وغير نيوتوني من خلال إتساع محوري مفاجئ، من خلال تغيير معايير التدفق مثل عدد رينولدز وعدد العائد. بحثت هذه الدراسة، التي أجريت باستخدام البرنامج ANSYS Fluent، في تأثير هذه المعلمات على هيكل تدفق السوائل. كشفت النتائج العددية أن مناطق إعادة التدوير لها طول وشدة تتناسبان مع عدد رينولدز، بينما تتناسب عكسيًا مع عدد العائد. بالإضافة إلى ذلك، يزداد معامل فقدان الضغط المحلي للسائل النيوتوني، وهو تأثير يتجلى أيضًا في حالة السائل اللزج. تم تطوير نماذج للتنبؤ بأطوال وشدة إعادة التدوير بالإضافة إلى معامل فقدان الضغط المحلي لكلا النوعين من السوائل.

الكلمات المفتاحية: السائل اللزج البلاستيكي- توسيع مفاجئ -سائل بينغهام - المِعْيارِ القانوني- إعادة التدوير-مناطق الدوامات - معامل فقدان الضغط.